DOE/ER/13467--T.

DOE/ER/13467--T1

DE87 012101

HYDROTHERMAL BRECCIATION IN THE JEMEZ FAULT ZONE, VALLES CALDERA, NEW MEXICO--RESULTS FROM CSDP COREHOLE VC-1

Jeffrey B. Hulen and Dennis L. Nielson

University of Utah Research Institute

Salt Lake City, Utah

FG02-86ER13467

Short Title: Hydrothermal Brecciation, Valles Caldera

June 1987

DISCLAIMER

ABSTRACT

Paleozoic and Precambrian rocks intersected deep in Continental Scientific Drilling Program corehole VC-1, adjacent to the late Cenozoic Valles caldera complex, have been disrupted to form a spectacular breccia sequence. The breccias are of both tectonic and hydrothermal origin, and probably formed in the Jemez fault zone, a major regional structure with only normal displacement since mid-Miocene. Tectonic breccias are contorted, crushed, sheared, and granulated; slickensides are common. Hydrothermal breccias, by contrast, lack these frictional textures, but are commonly characterized by fluidized matrix foliation and prominent clast rounding. The VC-1 hydrothermal breccias are intensely altered to quartz-sericite (illite ± phengite)-pyrite aggregates, locally accompanied by traces of sphalerite, chalcopyrite and molybdenite, and are cut by multiply intersecting quartz veinlets. Fluid inclusions in the hydrothermal breccias are dominantly two-phase, liquid-rich at room temperature, principally secondary, and form two distinctly different compositional groups. Older inclusions, unrelated to brecciation, are highly saline and homogenize to the liquid phase in the temperature range 189-246°C. Younger inclusions, in part of interbreccia origin, are low-salinity and homogenize (also to liquid) in the range 230-283°C. Vapor-rich inclusions locally trapped along with these dilute liquid-rich inclusions document periodic boiling. These fluid-inclusion data, together with alteration assemblages and textures as well

as the local geologic history, have been combined to model hydrothermal brecciation at the VC-1 site. Hydrothermal breccias form in active geothermal systems when total fluid pressures exceed the least principal effective stress, $sigma_x$, by an amount equal to the tensile strength, T, of the affected rock. For systems in extensional stress fields, such as prevailed during the VC-1 brecciation, $sigma_x$ is approximately equal to one third the lithostatic load, S_z, less hydrostatic fluid pressure, P, at the boiling point. The critical pressure required to hydrofracture, P_{fr}, is provided by the equation:

$$P_{fr} = (S_z - P)/3 + T$$

Boiling point vs. depth curves based on P_{fr} values graphically define the physical conditions of hydraulic rock rupture. Increasing vapor pressure beyond P_{fr} at a given depth, due to rapid release of confining pressure or renewed heating, will induce rock failure by hydrofracturing.

INTRODUCTION

Hydrothermal breccias are common features of active, high-temperature geothermal systems and their fossil equivalents, epithermal ore deposits. These breccias and associated hydraulic fracture networks not only focus thermal fluid flow, but are also important ore hosts (Sillitoe, 1985). In the active Waiotapu system, New Zealand (Hedenquist and Henley, 1985), ore-grade precious-metal precipitates are presently forming in hot-spring pools occupying phreatic explosion craters--the surface expressions of deeper hydrothermal brecciation. Hydraulic breccias and stockworks are also the principal ore hosts in hot-spring type gold orebodies (Berger, 1985; Lehrman, 1987), and are frequently encountered in deeper epithermal deposits (Fournier, 1983). Both geothermal and precious-metal exploration and development should benefit from a clearer understanding of the physical processes governing hydraulic rock rupture.

Molybdenite-bearing hydrothermal breccias discovered deep in Continental Scientific Drilling Program (CSDP) corehole VC-1, just southwest of the Valles caldera complex in north-central New Mexico (Figure 1), provide an excellent

Figure 1 near here

opportunity to characterize hydrothermal brecciation in the major outflow plume of a long-active, caldera-hosted, high-temperature geothermal system (Goff and Grigsby, 1982; Goff et al., 1986). This system has been extensively explored by a series of deep,

rotary geothermal wells (Union Oil Company (UOC), 1982). The cuttings recovered from these wells, however, provide only scant information about the faults, fractures, and probable breccias intersected at depth. Detailed study of continuous core from the hydrothermally brecciated rocks of VC-1, therefore, should also improve our understanding of intracaldera structural controls on deep thermal fluid flow.

The VC-1 hydrothermal breccias host abundant fluid inclusions, many of which apparently were trapped during brecciation. Homogenization temperatures and corresponding freezing-point depressions for these inclusions, when combined with alteration mineralogy and paragenesis as well as the inferred geologic history at the VC-1 site, allow development of a model of hydrothermal brecciation which should be broadly applicable in similar settings worldwide.

METHODS AND PROCEDURES

Characterization of the deep VC-1 breccias began with detailed lithologic logging of core from the lower 50 m of the corehole and progressed through petrographic examination, X-ray diffraction (XRD) analysis, and fluid-inclusion studies. Samples selected for XRD, nominally at 1.5 m intervals, were prepared for bulk analysis by light crushing, then hand-grinding a representative 1 g split in acetone to <325 mesh (<42 microns). These finely-ground samples were irradiated at $2^{o}2\theta$ from 2^{o} to $65^{o}2\theta$ using a Phillips diffractometer with CuK radiation source,

theta compensating slit, 0.2 mm (1/2°) receiving slit and focusing monochromator. Instrument settings were as follows: accelerating voltage--40 KV; tube current--40 mA; time constant--1/2 s; full-scale deflection--2500 counts per s; chart speed--25.4 mm/min. Approximate weight percentages of minerals identified on corresponding diffractograms were determined by comparing diagnostic peak intensities with those of standard phases, with appropriate corrections for matrix absorption. Clay fractions (<5 microns for this study) were extracted from the lightly crushed bulk samples by acoustic disaggregation in deionized water, Stokes' Law settling, and centrifugation. The resulting slurries were smeared on glass slides and irradiated at 1°2θ per minute after each of the following treatments: air-drying (2-37°2θ); vapor glycolation at 60°C for 24 hr (2-22°2θ); heating at 250°C for 1 hr (2-15°2θ); and heating at 550°C for 1 hr (2-15°2θ). Instrument settings were the same as for the bulk scans except for the time constant, maintained at 1 s. Approximate percentages of layer silicates identified on diffractograms corresponding to the above treatments were determined by reference to calibration curves (diagnostic peak intensity vs. weight percent) previously prepared using standard phases mixed in various proportions.

Whenever possible, the expandable interlayer content of illite and mixed-layer illite/smectite in the VC-1 clay fractions was determined using the methods of Srodon (1980). The less accurate, but more generally applicable techniques of Reynolds

(1980) were used to calculate this value when peak overlap due to contamination by non-clay phases precluded use of the Srodon method. On selected test samples, expandable interlayer contents determined by both methods were separated by no more than 10%.

Samples for fluid-inclusion analysis were prepared by doubly polishing rock chips 200-400 microns in thickness and 5-10 mm in diameter. Homogenization temperatures and freezing point depressions of fluid inclusions in these chips were measured using a Fluid Inc. modified U.S.G.S. gas-flow heating/freezing system. Slow heating rates (0.5°C/min. or less) and careful calibration ensured optimum accuracy and reproducibility (±0.2°C).

GEOLOGIC SETTING

Corehole VC-1 is located immediately southwest of the Valles caldera complex (Figure 1), comprising the 1.12 Ma Valles caldera (Self et al., 1986), its spatially coincident predecessor, the 1.45 Ma Toledo caldera (Self et al., 1986; Heiken et al., 1986), and possibly small precursor calderas formed at the same site between 3.6 and 1.45 Ma (Nielson and Hulen, 1984; Self et al., 1986). Calderas of the Valles complex represent the culminating volcanic episode in the Jemez volcanic field, active since at least 16 Ma (Gardner et al., 1986) at the western margin of the northerly-trending Rio Grande Rift. The Jemez field appears to have been localized by the intersection of this rift boundary with the Jemez lineament, a regional feature trending northeast

and defined by alignment of Cenozoic volcanic centers and major structures such as the Jemez fault zone (Figure 1; Laughlin, 1981).

Evolution of the Valles caldera complex was probably underway by 3.6 Ma, when low-volume, felsic ash-flow tuffs began erupting near the center of the Jemez volcanic field (Self et al., 1986). Expulsion of these tuffs probably led to development of a small caldera or set of calderas now completely concealed by Valles caldera fill (Nielson and Hulen, 1984; Self et al., 1986). Felsic ignimbrites aggregating approximately 300 km^3 in volume were violently ejected at 1.45 Ma, resulting in emplacement of the Otowi Member of the Bandelier Tuff and formation of the Toledo caldera (Doell et al., 1968; Izett et al., 1980; Self et al., 1986). At 1.12 Ma, a second major felsic pyroclastic eruption of roughly equivalent volume produced the Tshirege Member of the Bandelier Tuff (Izett et al., 1980; Self et al., 1986). The Tshirege eruption destroyed most of the Toledo caldera but resulted in formation of the Valles caldera at essentially the same site (Heiken et al., 1986). Collapse of the Valles caldera was followed shortly by resurgent doming. The apical graben of the resurgent Redondo dome and the ring-fracture zone of the Valles caldera ("structural margin" on Figure 1) subsequently guided emplacement of rhyolite domes and flows until about 0.13 Ma (Gardner et al., 1986).

VC-1 is collared just southwest of the intersection of the Valles caldera's structural margin with the subsurface projection

of the Jemez fault zone (Figure 1). A major crustal flaw since perhaps Pennsylvanian time (J. N. Gardner, pers. comm., 1986), the Jemez fault zone not only controls the location of the apical graben of the Valles caldera's resurgent dome, it also focuses the southwesterly-flowing hydrothermal plume draining the caldera's active geothermal systems (Goff et al., 1986). Since mid-Miocene, the Jemez fault zone has been characterized by exclusively normal displacement; prior strike-slip movement, however, is locally evident (Aldrich and Laughlin, 1984).

Valles caldera geothermal systems, fueled by cooling, subcaldera plutons, were explored by Union Oil Company (UOC; now Unocal) between 1971 and 1982 (UOC, 1982). UOC concentrated its exploration efforts on the two areas of highest heat flow and most intense surficial alteration in the Valles caldera--the Redondo Creek graben and the Sulphur Springs area, near the western structural margin (Figure 1). Liquid-dominated conditions prevail below a nominal depth of 500 m in both areas. Hydrothermal fluids in this regime are high-temperature (up to about 300°C), neutral-chloride waters ranging from 5000 to 18,000 mg/Kg total dissolved solids (Truesdell and Janik, 1986; Shevenell et al., 1987); temperatures up to 341°C have been recorded in impermeable rocks beneath the hydrothermal system (Nielson and Hulen, 1984).

Circulating in permeable faults, fractures, and breccias as well as discrete sandstone and non-welded tuff horizons (e.g. Hulen and Nielson, 1982), thermal fluids of the Valles caldera

have interacted with their host rocks to form distinct alteration assemblages (Hulen and Nielson, 1986a, 1986b; Hulen et al., in press). Intense phyllic (and locally potassic) alteration is diagnostic of principal fluid conduits; propylitic alteration prevails away from these channels. Water vapor is now the pressure-controlling fluid to a an average depth of about 500 m, but a shallow, widespread cap of mixed-layer illite/smectite indicates that the liquid-dominated reservoir once extended up to (and probably above) the present ground surface. This conclusion is corroborated by the occurrence of near-surface molybdenite-quartz-fluorite mineralization in the Sulphur Springs area (Hulen et al., in press). Only a veneer of scattered, acid-sulfate advanced argillic alteration, concentrated at Sulphur Springs (Goff and Gardner, 1980; Charles et al., 1986) is related to contemporary, shallow, vapor-dominant conditions.

Active geothermal systems of the Valles caldera are clearly analogues of fossil systems responsible for depositing various epithermal ores. Hulen and Nielson (1986a, 1986b) noted numerous parallels between the active Valles systems and those which formed Creede-type, epithermal silver/base metal deposits. Hulen et al. (in press) documented unique, sub-ore grade, epithermal molybdenite mineralization in <1.12 Ma tuffs penetrated in CSDP corehole VC-2A, at Sulphur Springs (Figure 1). This occurrence, along with traces of molybdenite in the VC-1 hydrothermal breccias discussed in this paper, may be the near-surface expression of deeply-concealed, Climax- or granite-type

molybdenum mineralization (e.g. White et al., 1981; Mutschler et al., 1981).

Figure 2 is a generalized stratigraphic and temperature log for VC-1. To a depth of 333 m, the hole penetrates post

Figure 2 near here

-Bandelier rhyolite flows, tuffs, and breccias ranging in age between 0.13 Ma and 0.60 Ma (Gardner et al., 1986; J. Gardner and F. Goff, pers. comm., 1986). Beneath this young volcanic sequence, redbeds of the Permian Abo Formation extend to a depth of 424 m. Two Pennsylvanian formations were intersected--the Madera Limestone, a dominantly marine carbonate sequence between 424 and 809 m; and the Sandia Formation, a near-shore, calcareous siliclastic unit extending to a depth of 826 m.

This paper focuses on the lower 30 m of VC-1 (Figure 2), an extremely complex interval comprising deformed and brecciated, hydrothermally altered, Paleozoic sedimentary rocks and Precambrian gneiss. The extreme disruption of these rocks, together with the location of VC-1 (Figure 1), strongly suggests that the bottom of the corehole penetrates a subsurface extension of the Jemez fault zone.

An important objective in drilling VC-1 was characterization of an active geothermal outflow plume near its source (Goff et al., 1986). Although measured temperatures in the corehole do not exceed 160°C (Figure 2), we will present evidence from the

deep hydrothermal breccia zone that the Valles plume attained temperatures approaching 300°C in the geologically recent past.

STRATIGRAPHY

Much of the VC-1 breccia zone, spanning the depth interval 826.2-856.1 m and detailed in Figure 3, is so

Figure 3 near here

thoroughly disrupted and altered that its components cannot be ascribed to particular stratigraphic units. Portions of the zone, however, are sufficiently intact that relict texture and mineralogy can be used for identification. In this section, we will briefly describe these relatively undisturbed rocks and attempt to correlate them with formally designated formations in north-central New Mexico, but primarily as a framework for discussing the spectacular breccias they host.

The deepest VC-1 rock unit that can be correlated confidently with a regional counterpart is the Precambrian gneiss intersected between depths of 841.8 and 844 m (Figure 4). Although highly fractured, quartz-sericitized, and cut

Figure 4 near here

by numerous hydrothermal veinlets, this rock is still recognizable as a weakly foliated, medium-crystalline, granitic orthogneiss. The rock is texturally identical to the unaltered gneiss penetrated below a depth of 3115 m in UOC borehole B-12, about 5 km to the northeast in the Valles caldera (Figure 1). It

is also very similar to gneiss in the nearest Precambrian exposure, near Soda Dam (Figure 1). In thin-section, the VC-1 gneiss is seen to be so thoroughly disrupted that it actually consists of rock "islands" separated by thin rock-flour septa or hydrothermal veinlets. Thus it is technically a breccia. However, clasts generally account for greater than 95 volume percent, and the parentage of the rock is readily recognizable; therefore, it will be referred to simply as gneiss.

The gneiss "islands" noted above consist of polycrystalline quartz aggregates, commonly granoblastically recrystallized, intergrown with weakly to strongly sericitized microcline and orthoclase as well as stubby lath-shaped sericite aggregates replacing primary plagioclase. "Sericite" in this case and throughout this paper refers to fine-crystalline illite as well as phengite, a gray-green, iron-rich, illite analogue. The Precambrian gneiss also contains up to 3% relatively coarse-crystalline (1-2 mm diameter) mica, principally muscovite with traces of feebly pleochroic light brown biotite. Apatite, zircon, sphene, rutile, and hematite (replacing magnetite or ilmenite) are present in trace amounts.

Resting unconformably on the orthogneiss in VC-1 is a well-bedded, fine- to medium-grained quartz sandstone 3.3 m in thickness (Figure 3). Semi-quantitative bulk XRD analysis shows that this sandstone is approximately 92% (wt.) quartz, with 2% pyrite and 6% illite; petrographic examination reveals the additional presence of traces of detrital potassium feldspar.

Most of the quartz is concentrated in detrital grains, but some occurs as a fine-crystalline cement. The illite is principally interstitial, and probably initially authigenic or diagenetic, but has recrystallized hydrothermally.

The quartz sandstone is overlain by 3.1 m of fine- to coarse-crystalline, stylolitic and locally laminated limestone (Figure 3). Consisting principally of calcite (92-95%), this limestone also contains minor (5%) detrital quartz; traces of illite, chlorite, and pyrite are concentrated in stylolites.

Both the stylolitic limestone and underlying quartz sandstone may represent the Espiritu Santo Formation of the Mississippian Arroyo Penasco Group (Armstrong and Mamet, 1974). Wherever observed in north-central New Mexico, the Espiritu Santo Formation comprises a basal clastic horizon, the Del Padre Sandstone Member, resting unconformably on Precambrian basement rock, and an overlying carbonate sequence.

Clasts in a complexly brecciated and altered interval between depths of 831.3 and 835.4 m, immediately above the stylolitic limestone (Figure 3), are of unknown stratigraphic affiliation. This breccia zone and others deep in VC-1 will be discussed in detail in the following section on tectonic and hydrothermal brecciation.

A distinctive, hematitic, rebrecciated sedimentary breccia spans the depth interval 826.3-831.3 m (Figure 3). This distinctive rock, originally a chert-bearing redbed, will also be described in more detail in the following section. The salient

primary features of this unit are its brick-red, hematitic, argillaceous to sandy matrix and abundant, angular chert clasts (Figure 5). Diagenetic illite

Figure 5 near here

and chlorite, locally hydrothermally recrystallized, are the principal matrix constituents.

Assuming that the Precambrian gneiss in VC-1 is overlain by the Mississippian Espiritu Santo Formation, as discussed above, the chert-bearing redbed breccia may represent the overlying Log Springs Formation, of uppermost Mississippian age (Armstrong and Mamet, 1974). At the type locality in the southwestern Nacimiento Mountains, about 30 km southwest of VC-1, the Log Springs Formation consists of hematitic shale, sandstone and conglomerate; coarser clastic units contain angular to rounded pebbles of Mississippian chert and limestone as well as Precambrian gneiss and schist. At Guadalupe Box, only about 16 km southwest of VC-1, the formation is entirely red ferruginous shale (DuChene, 1974). The iron-rich character and brick-red coloration of the Log Springs formation throughout north-central New Mexico is believed to indicate deposition of the unit as a residual soil or regolith (Armstrong and Mamet, 1974).

Between depths of 809.2 and 826.3 m, immediately above the presumed Log Springs Formation, VC-1 penetrated a dominantly siliciclastic sequence believed to be the Pennsylvanian Sandia Formation (Figure 3; Gordon, 1907; Kelley and Northrop, 1975). Like the Sandia Formation throughout northern New Mexico, this

sequence appears to have been deposited in a rapidly fluctuating marine shoreline environment (DuChene, 1974; Siemers, 1983; Baltz and Myers, 1984). The upper contact of the Sandia in VC-1 with the overlying Pennsylvanian Madera Limestone is characteristically transitional. The boundary between the two formations in the corehole is arbitrarily placed, as suggested by Loughlin and Koschmann (1942), at the top of a prominent sandstone above which limestones are predominant and below which terrigenous strata are more prevalent.

Calcareous quartz sandstone, shaly limestone and shale are the principal lithologies of the VC-1 Sandia Formation (Figure 3). Layer silicates are locally abundant in these rocks, particularly in shaly horizons; illite-rich, mixed-layer illite/smectite is predominant, but iron-rich chlorite is also common. The illite/smectite is principally of diagenetic origin (see also Keith, this issue), but within and adjacent to more permeable zones in the Sandia Formation is hydrothermally recrystallized; post-Sandia hydrothermal illite/smectite occurs locally as a vein- and vug-filling phase. Chlorite in the Sandia formation is also of both diagenetic and hydrothermal origin.

TECTONIC AND HYDROTHERMAL BRECCIAS

Introduction

The Paleozoic and Precambrian sequence discussed above is disrupted, below a depth of 826.3 m, into a spectacular breccia sequence (Figure 3) of both tectonic and hydrothermal origin.

Before characterizing each of the major breccias in this sequence, we will briefly discuss the textural evidence for their genesis, hopefully aiding breccia recognition in core and outcrop elsewhere.

Tectonic breccias are texturally distinct from those developed hydrothermally, although gradational varieties can be difficult to identify with confidence. Textures of tectonic breccias reflect their cataclastic origin; original rocks are brittly fragmented, with rotation of clasts, frictional grain boundary sliding and granulation (Sibson, 1977), and commonly production of slickensides. Hydrothermal breccias, by contrast, ideally lack these frictional textures, displaying instead those indicating an explosive origin.

Two end-member varieties of hydrothermal breccia are common in both active and fossil geothermal systems--"jigsaw-puzzle" breccias and those that have undergone fluidization. Jigsaw-puzzle breccias, such as those of the Waiotapu geothermal system, New Zealand (Hedenquist and Henley, 1985) are created by explosive, three-dimensional, hydraulic expansion of a fractured host rock. This expansion may be accompanied by forceful ejection of fragments into an open fissure (e.g. Grindley and Browne, 1976). Fragments in these breccias are typically subangular to angular, minimally rotated, and only slightly displaced from their points of origin. The matrix, comprising smaller fragments, rock flour, and hydrothermal phases in various

proportions, shows no evidence of crushing or shearing unless modified by subsequent tectonic activity.

Textures of fluidized breccias provide evidence of their formation in a more energetic hydrothermal regime. Fluidization involves suspension, abrasion, and sometimes entrainment and transport of rock fragments in a highly overpressured, outward-escaping gas or liquid stream (Reynolds, 1954; McCallum, 1985) which may or may not vent to the surface. Fragments in fluidized breccias, depending on the degree of transport and attrition, may be angular to extremely well-rounded. The matrix is commonly flow-foliated, with both lamellar and turbulent foliation locally present. Neither matrix nor clasts, however, unlike their counterparts in tectonic breccias, are crushed, granulated, sheared, or disrupted by slickensides.

If used in conjunction with the textural criteria presented above, hydrothermal alteration itself may help deduce the origin of a breccia. Breccias developed hydrothermally are more likely to be altered than tectonic breccias, since their formation requires the same fluids responsible for alteration. Furthermore, the pressure release accompanying hydrothermal brecciation may induce boiling, a process highly conducive to alteration and mineralization (Fournier, 1983).

Breccias of VC-1

Deep tectonic and hydrothermal breccias in VC-1 almost certainly developed in a branch of the Jemez fault zone (Figure

1). The corehole is collared directly above the subsurface northeastern extension of this structure, and major tectonic displacement of the VC-1 rocks is indicated by the occurrence of contorted, probable Paleozoic shale stratigraphically beneath Precambrian basement rock (Figure 3). Jemez fault breccias probably transmitted and accumulated the overpressured fluids responsible for subsequent hydrothermal brecciation.

The VC-1 breccias are concentrated in two intervals. The deepest interval, between 844 m and 856.1 m (Figure 3), includes a basal zone of contorted and fractured shale, a overlying, multilithologic tectonic breccia, and a molybdenite-bearing hydrothermal breccia. The upper breccia interval, spanning the interval 826.3-835.4 m and including redbeds of the Log Springs Formation (?) is a complex sequence we believe to be tectonically and hydrothermally rebrecciated sedimentary breccia.

In addition to the disturbed Log Springs (?) interval, the upper breccia zone in VC-1 includes two heterolithologic breccias intersected in the intervals 831.3-832.7 m and 834.0-835.4 m (Figure 3). These breccias, separated by a monlithologic, brecciated limestone, contain approximately 50% (vol.) angular to highly rounded clasts, up to at least 20 cm (avg. about 2 cm) in diameter, embedded in a chloritic to locally siliceous and calcareous, silty to sandy matrix which locally is turbulently flow-foliated. The clasts comprise, in decreasing order of abundance: sandstone and siltstone; chert; massive, fine-crystalline chlorite;

partially dolomitized and mineralized limestone and limestone breccia (Figure 6); hydrothermal quartz crystal fragments and

Figure 6 near here

aggregates; and rare pyrite. The two breccias are separated by a 1.5 m-thick intercept of limestone breccia. This rock consists of mostly angular, subsequent clasts of medium-crystalline calcite, averaging about 2 cm in diameter, embedded in a texturally and compositionally identical matrix.

These two breccia intervals and intervening brecciated limestone almost certainly had complex multiple origins. We have tentatively identified the overlying chert-bearing hematitic breccia (Figure 3) as the Mississippian Log Springs Formation, probably a red soil or regolith developed on underlying carbonate strata. The subjacent breccias under discussion, then, could have formed initially by collapse during contemporaneous solution activity in underlying Mississippian carbonates. However, mineralized Paleozoic carbonate clasts and delicate, non-eroded hydrothermal quartz crystal fragments indicate that these breccias were probably modified well after the Paleozoic--there are no reported Paleozoic hydrothermal events in the Jemez Mountains (e.g. Gardner, 1986).

Clast rounding and turbulent flow-foliation in these breccias suggest that they may have been modified by hydrothermal fluidization. The porous, karstic network in which the breccias may have formed initially would provide excellent conduits for the escape of overpressured hydrothermal fluid. This fluid

streaming would facilitate hydrothermal alteration and redistribution of original collapse debris.

Primary characteristics of the chert-bearing, brecciated redbed believed to be the Mississippian Log Springs Formation between 826.3 m and 831.3 m (Figures 3 and 5) were discussed in a previous section. A number of secondary features lead us to believe that this unit has also been rebrecciated. Both the matrix and clast margins show evidence of crushing, shearing, and granulation (Figure 5), and slickensides are abundant. Clasts are commonly hydrothermally altered and mineralized; chert breccia clasts have been multiply re-brecciated and quartz-veined (Figure 5). The matrix of this redbed breccia also contains delicate, sharply-faceted hydrothermal quartz crystal fragments, which could not have survived in their unabraded condition during normal sedimentary transport and deposition. All these features, taken together, lead us to believe that at the VC-1 site, the Log Springs Formation has been extensively disrupted by faulting along the Jemez fault zone.

By contrast with the breccias of the upper zone in VC-1, those of the lower zone, between 844 m and 856.1 m (Figure 3) have unambiguous origins. The basal fractured shale and overlying, carbonate-rich breccia are clearly tectonic features. The overlying, molybdenite-bearing breccia was formed hydrothermally.

The contorted shale intersected at the base of the lower breccia zone, between depths of 852.6 m and 856.1 m (Figure 3),

is basically a quartz-illite rock with minor pyrite and chlorite. As in overlying sedimentary rocks, Much of the layer silicate fraction is probably authigenic or diagenetic in origin. Both illite and chlorite, however, have been extensively recrystallized, and illite microveinlets are locally common. This shale is thoroughly disrupted. Individual laminae can be traced only a few cm; slickensides and randomly oriented fractures are abundant. The shale is of unknown stratigraphic affiliation. However, since it was intersected beneath Precambrian gneiss, its present position in VC-1 must reflect post-depositional displacement. The gneiss most likely was moved above the shale by reverse or strike-slip faulting along the Jemez fault zone prior to mid-Miocene (the beginning of the current episode of normal displacement; Aldrich and Laughlin, 1984). Alternatively, the gneiss could have been emplaced above the shale by gravity sliding.

Shaly, carbonate-rich, tectonic breccia overlies the basal shale and spans the interval 849.5-852.6 m (Figures 3 and 7). This breccia consists of 10-20% (vol.) subrounded to

Figure 7 near here

angular clasts, averaging about 4 mm (up to 3 cm) in diameter, in a silty, argillaceous, commonly sheared and foliated matrix. The clasts comprise sandstone, siltstone, limestone and chert as well as altered hydrothermal breccia and Precambrian gneiss (Figure 7) derived from immediately overlying units.

Intensely altered, locally molybdenite-bearing hydrothermal breccias were penetrated in VC-1 between depths of 844 m and 849.5 m (Figure 3), immediately beneath similarly altered Precambrian gneiss. These breccias, distinctively bright gray-green in color due to phengitic alteration, consist of angular to highly-rounded clasts, up to 5 (avg. about 1.5) cm in diameter, embedded in a locally flow-foliated rock-flour matrix (Figures 8 and 9).

Figures 8 and 9 near here

The clasts represent Precambrian orthogneiss, quartz-rich sandstone, polycrystalline hydrothermal vein quartz, and minor chert, as well as older breccias formed of one or more of these components. Relict sedimentary quartz grains in sandstone clasts commonly are surrounded by secondary quartz overgrowths, from which they are separated by rings of solid and fluid inclusions. The matrix of the breccia locally incorporates sand-size quartz clasts, probably derived in part by sandstone disaggregation.

Several textural features, considered together, suggest that these molybdenum-bearing phengitic breccias were developed by hydrothermal rather than tectonic processes. First, the general absence of slickensiding, shearing, crushing and granulation (slickensides on a few late-stage molybdenite veinlets are a notable exception) strongly argues against their formation as fault breccias. Secondly, clasts commonly appear abraded, and many are highly rounded (Figures 8 and 9), features which could indicate attrition during fluidization. Also the matrix locally

displays both lamellar and turbulent flow foliation (Figure 9), another feature indicative of hydrothermal gas-streaming. Portions of the breccia show a well-developed jigsaw-puzzle texture, discussed in the introduction to this section. Finally, these breccias are intensely altered, possibly by the fluids responsible for hydrothermal brecciation.

HYDROTHERMAL ALTERATION

The entire pre-volcanic sequence penetrated by VC-1 is either diagenetically or hydrothermally altered to a greater or lesser degree. Most affected is the molybdenite-bearing hydrothermal breccia discussed immediately above. Scattered intervals of strong alteration and veining throughout the Paleozoic sequence, however, attest to local interaction of the rock with high-temperature hydrothermal fluids. Diagenesis and hydrothermal alteration of the thick Madera Limestone and Sandia Formation are detailed by Keith (this issue). In this paper, we focus on alteration beneath the Sandia, principally in the complexly brecciated rocks described in the previous section.

The transition from dominantly diagenetic to principally hydrothermal regimes in the rocks penetrated by VC-1 appears to coincide with the contact between the Pennsylvanian Sandia Formation and the Mississippian Log Springs Formation (?) (Figure 3). Above this contact, semi-quantitative bulk XRD analysis shows that the clay fraction is dominated by mixed-layer illite/smectite with subordinate chlorite. The illite/smectite

is a highly ordered variety with 10-15% expandable (smectite) interlayers. Below the contact, illite with less than 5% expandable interlayers is the principal layer silicate. Numerous investigators (e.g. Dunoyer de Segonzac, 1970) have shown that the interlayer smectite content of illite/smectite is a temperature-sensitive variable. The downward transition from illite/smectite in the Sandia shales to illite in the Log Springs (?) redbeds, however, seems too abrupt to reflect simply a normal geothermal gradient in a deep sedimentary basin. There are at least two explanations for this sharp transition: tectonic disruption has juxtaposed formerly separate lower- and higher-grade diagenetic facies, or the expandable interlayer smectite content of the illite/smectite in the brecciated Log Springs (?) Formation has decreased through contact with (or conductive heating induced by) circulating hydrothermal fluid.

The upper breccia interval (826.3-835.4 m; Figure 3) in VC-1 shows evidence of both pre- and post-breccia hydrothermal alteration. Clasts in all three major breccia zones in this interval are commonly altered and hydrothermally veined, with alteration textures and veinlets truncated at clast boundaries (Figure 5). The breccias also incorporate delicate hydrothermal quartz crystal fragments. The breccia intersected between depths of 831.3 m and 832.7 m also hosts mineralized carbonate (limestone/dolomite) and carbonate breccia clasts which contain highly variable amounts of disseminated and veinlet-controlled magnetite, hematite and pyrite. A few of these carbonate clasts

also contain disaggregated, coarse-crystalline barite (Figure 6). In addition to this pre-breccia alteration, the rocks of the upper breccia interval in VC-1 are also sparsely cut by chlorite ± calcite microveinlets and very rarely by pyrite microveinlets; pyrite also locally replaces carbonate clasts. The breccia intersected in the interval 831.3-832.7 m is also cut by veinlets and irregular masses of chlorite with minor quartz and calcite. All three alteration minerals were probably formed during Keith's (this issue) hydrothermal stage I, at temperatures of 200 # 25°C.

Precambrian gneiss and underlying, molybdenite-bearing hydrothermal breccia are the most intensely altered units intersected in VC-1. Original rock plagioclase in the gneiss is totally altered to fine-crystalline illite and. Primary sphene and perhaps ilmenite are altered to microcrystalline leucoxene. Biotite is replaced by iron-rich chlorite, and may also be represented by disseminated muscovite pseudomorphs. Accessory, primary iron oxides are widely replaced by brick-red hematite. Traces of primary apatite and zircon remain unaffected. The gneiss is also cut by numerous veinlets of quartz, quartz-sericite, quartz-phengite and quartz-sericite-phengite, all of which contain minor pyrite. The veinlets are multiply cross-cutting (Figure 4). Quartz-sericite ± pyrite veinlets, the earliest formed, are cut by quartz-phengite ± sericite ± pyrite veinlets, which in turn are cut by quartz ± pyrite veinlets. The early veinlets may represent Keith's (this issue) hydrothermal stage II, with an upper temperature limit, at this depth, of

about 275°C. Subsequent veinlets in the gneiss probably formed during separate pulses of Keith's (this issue) stage III alteration, which on the basis of phengite occurrence in other active hydrothermal systems she suggests may have occurred at temperatures approaching 300°C. These results are consistent with paleotemperatures we have obtained from analysis of fluid inclusions in quartz veinlets cutting the gneiss and underlying hydrothermal breccia.

The phengitic hydrothermal breccias (844-849.5 m; Figure 3) are so intensely altered that no primary rock feldspar remains. Both clasts and matrix in these breccias are converted completelyto quartz-illite-phengite-chlorite-pyrite aggregates locally incorporating minor calcite; primary quartz along with traces of apatite and zircon remain as relict phases. Phengite is much more abundant than in the overlying gneiss, imparting to the breccias a vivid gray-green coloration.

Hydrothermal veinlets are less abundant in these breccias, but as in the overlying gneiss comprise various combinations of quartz, illite, phengite and pyrite; traces of chalcopyrite and sphalerite are locally present. Age relationships among veinlets are more ambiguous than in the gneiss, but in general, quartz-sericite veinlets are earliest and phengite-bearing veinlets late-stage. Many veinlets in clasts are abruptly cut off at clast margins (Figure 9), clearly indicating development prior to brecciation. Other veinlets, particularly those rich in quartz relative to illite and phengite, transect clasts and older

matrix, but abruptly terminate against younger matrix. We interpret this relationship to indicate formation of the veinlets during a brief pause in the brecciation--that is, they are interbreccia features.

Pyrite is overall the most abundant sulfide in these phengitic hydrothermal breccias, overall accounting for about 1% (wt.) of the rock (Figure 3), but locally reaching concentrations of 3-5% in scattered 1-5 cm intervals. Pyrite deposition almost certainly accompanied each pulse of hydrothermal brecciation and alteration. The pyrite occurs principally as disseminated, generally subhedral grains and grain aggregates averaging about 1 mm (up to 3 mm) in diameter, but also in microveinlets with or without quartz, seicite and phengite. The veinlet pyrite is accompanied by rare local traces of texturally similar but extremely fine-crystalline (<0.1 mm in diameter) chalcopyrite and sphalerite.

Molybdenite is also present in the phengitic hydrothermal breccias, and appears to have been the most recent sulfide deposited. Principally confined between depths of 845.8m and 847.5 m (Figure 3), the molybdenite occurs as thin, discontinuous films on phengite-coated fractures, and on the surfaces of scattered clasts. We were unable to obtain enough of the molybdenite for complete characterization by XRD, but its identity was confirmed by SEM analysis. The sulfide has the submetallic appearance and typical blue-gray sheen of the 2H polymorph, characteristic of stockwork molybdenum deposits such

of the nearby Questa caldera in northern New Mexico (Leonardson et al., 1983).

At least five stages of alteration and mineralization in these breccias are suggested by cross-cutting and replacement textures. During an early stage, possibly corresponding to Keith's (this issue) stage I, quartz-rich sandstone and Precambrian granitic gneiss were replaced by quartz + chlorite ± sericite and pyrite, then flooded (sandstone only) and veined with coarse, polycrystalline quartz, and finally tectonically or hydrothermally brecciated. The rock-flour matrix of the newly-formed breccia was further altered to quartz and micaceous illite with minor pyrite (Keith's stage II?). This altered rock was hydrothermally rebrecciated, with attendant fluidization. The matrix and some clasts in this late breccia were replaced by quartz, sericite, pyrite, and phengite during several pulses possibly representing Keith's (this issue) alteration stage III. During each pulse, fractures in the breccia, at least partially hydraulic in origin, were filled by quartz veinlets also containing variable amounts of illite, phengite and pyrite. Sparse molybdenite mineralization accompanied or shortly followed phengitic alteration. The age of the molybdenite relative to late interbreccia quartz veinlets could not be determined.

FLUID INCLUSIONS

The deep hydrothermal breccias of VC-1 are riddled with small fluid inclusions that confirm the complex hydrothermal

history suggested by alteration mineralogy and texture (see also Sasada, this issue). As we will discuss in detail later in this section, the inclusions form distinct, low- and high-salinity compositional groups. Inclusions of both groups, however, are texturally identical, and can be distinguished only by heating and freezing experiments. The inclusions are principally secondary, occurring as planar aggregates and curviplanar "veils" which are randomly oriented and intersect to form web-like networks. Unambiguous primary inclusions are rare, low-salinity, and confined to probable interbreccia quartz veinlets. Microthermometric measurements of these low-salinity, interbreccia quartz veinlets are very similar to those of low-salinity secondary inclusions in quartz clasts. This relationship suggests that dilute primary and secondary inclusions could be in part coeval.

Secondary fluid inclusions in the VC-1 breccias are small, ranging from <0.2 microns to 11 microns in diameter, but averaging less than 1 micron in diameter. Highly irregular inclusions are most abundant, particularly among those larger than 3 microns in diameter, but elongate and equant varieties, some partially bounded by negative crystal faces, are also common. Most secondary inclusions are two-phase and liquid-dominated at room temperature, with vapor bubbles estimated to account for 5-15 volume percent. However, vapor-rich inclusions are also locally present. Many of these clearly reflect necking (Roedder, 1984), but others, particularly those concentrated with

liquid-rich, low-salinity inclusions along single planes, appear to have undergone minimal modification since trapping. These coexisting liquid- and vapor-rich inclusions are believed to indicate boiling. If as discussed above, the secondary low-salinity inclusions are genetically related to primary low-salinity inclusions in interbreccia quartz veinlets, then the boiling took place during hydrothermal brecciation.

The few definite primary inclusions identified are texturally similar to those of secondary origin, but are either arranged in non-planar three-dimensional arrays or attached to solid phases. They are invariably low-salinity, and range in diameter from <0.2-4 microns.

High- and low-salinity inclusions in the VC-1 breccias respond much differently to freezing procedures. High-salinity inclusions freeze abruptly upon supercooling to -65°C to -74°C, forming a dense, brownish, sub-translucent solid. They become conspicuously granular-appearing, probably due to the onset of melting, at about -50°C, and show definite melting by -40°C. Low-salinity inclusions, by contrast, freeze upon supercooling at -40°C to -45°C without discoloration; melting commences at about -28°C.

The very low initial melting point of high-salinity inclusions indicates that they contain appreciable calcium chloride or (much less likely) magnesium chloride in addition to sodium chloride (Roedder, 1984). For these inclusions, sodium chloride-based salinity values calculated using the methods of

Potter et al. (1978) must be considered quite approximate. The initial -28°C melting temperature for the low-salinity inclusions, however, indicates that they contain dominantly or exclusively sodium chloride waters (Roedder, 1984).

Homogenization temperatures and corresponding ice-melting temperatures (freezing-point depressions) were measured for 58 two-phase, liquid-dominated fluid inclusions in two hydrothermal breccia samples (from depths of 846 m and 846.7 m) and from hydraulically (?) fractured Precambrian gneiss at 842.9 m. Since ice-melting temperatures could be measured reliably in these samples only for inclusions larger than 2.5 microns in diameter, a bias in favor of larger inclusions could have been introduced. However, the distribution of homogenization temperatures for these larger inclusions is very similar to the temperature distribution for all inclusions regardless of size. This similarity suggests that the large inclusions are representative of those spanning the full size range.

The inclusions analyzed form distinct low- and high-salinity populations. These are clearly separated on a plot of homogenization temperatures vs. corresponding ice-melting temperatures (Figure 10). All but two of the 28 high-

Figure 10 near here

salinity inclusions show ice-melting temperatures between -16.5°C and -23.1°C, and homogenize to the liquid phase at temperatures ranging from 189.4°C to 245.7°C. By contrast, 30 of 31 low-salinity inclusions, with ice-melting temperatures tightly

confined between -0.1°C and -1.8°C, homogenize in a much higher temperature range between 229.5°C ad 283.9°C. Geologic evidence to be discussed in the following section strongly suggests that inclusions of the low-salinity group were trapped at shallow depth. Measured homogenization temperatures for these inclusions, therefore, are believed to be very close to trapping temperatures. The probable trapping depth range of the high-salinity inclusions is unknown. In both cases, we believe that pressure corrections (Potter, 1977) are unwarranted.

Shown for comparison with the VC-1 results on Figure 10 are homogenization temperatures for fluid inclusions in shallow (<1304 m depth) samples of Precambrian crystalline rock penetrated in a geothermal well at the nearby Fenton Hill Hot Dry Rock site (Figure 1; Burruss and Hollister, 1979). All but two of the Fenton Hill inclusions, many of which are extremely saline, homogenize at lower temperatures than those of VC-1. The two atypical Fenton Hill inclusions plot within the dilute, high-temperature VC-1 group (Figure 10), and conceivably could record the same hydrothermal episode. In general, however, the VC-1 inclusions trapped much higher-temperature hydrothermal fluids. This disparity probably reflects the relative ease with which these fluids could invade the more permeable rocks of the Jemez fault zone.

Fluid-inclusion data obtained for VC-1 have been plotted on an enthalpy-chloride diagram (Figure 11), often used to assess

Figure 11 near here

the origins of deep geothermal waters (Truesdell and Fournier, 1976). Fluids derived by boiling are represented on these diagrams as points along steam-loss lines radiating from the saturated steam point at 0% chloride and an enthalpy of 2775 KJ/Kg at 284°C. A dilution line similarly emanates from the chloride-enthalpy point for cold water (in this case assumed to be Jemez River water) and constrains fluid compositions possible through mixing. Figure 11 demonstrates that the high- and low-salinity inclusion fluids in the VC-1 breccias could not have developed from one another through boiling or dilution. Compositional differences within groups, however, could be due in part to either or both processes, and to subtle changes in reservoir conditions during the evolution of multiple hydrothermal systems. Coexisting low-salinity, liquid-rich and vapor-rich inclusions along scattered, healed microfractures suggest that these dilute fluids boiled during hydrothermal brecciation.

MODEL FOR HYDROTHERMAL BRECCIATION

The fluid-inclusion data discussed above can be combined with paragenetic information from alteration studies as well as the local geologic history to model hydrothermal brecciation at the VC-1 site. The model should have general application in similar settings elsewhere.

The following observations, presented in previous sections, are critical in formulating such a model. First, the breccias are developed in the structurally permeable Jemez fault zone. Second, the VC-1 site is immediately adjacent to the Valles caldera complex, and thus to a potent magmatic heat source. Finally, rounding of clasts and flow-foliation of the matrix suggests that the breccias were emplaced or modified by hydrothermal fluidization.

The absolute age of the VC-1 hydrothermal breccias is uncertain, since the youngest clasts are Paleozoic sedimentary rocks. In view of the hydrothermal history of the Jemez Mountains and the location of the VC-1, however, it is compelling to assume that these breccias are genetically related to the Valles caldera complex. Dated, post-Precambrian hydrothermal events in the Jemez Mountains are confined to the Late Cenozoic (e.g. Wronkiewicz et al., 1984; Gardner et al., 1986), so the age of hydrothermal brecciation and alteration at the VC-1 site is probably similarly constrained. Although each of the numerous volcanic episodes in the Jemez Mountains since about 16 Ma must have been accompanied by hydrothermal activity, only in the Valles caldera complex and in the Bland mining district, over 16 km southeast of VC-1, is there obvious evidence of this activity. Epithermal precious metal mineralization dated at about 6 Ma (Wronkiewicz et al., 1984) in the Bland district is accompanied by widespread propylitic and local argillic alteration, but hydrothermal breccias are apparently absent. By contrast, these

breccias appear to be widespread in the Valles caldera complex; each of the two Valles CSDP coreholes completed to date, VC-1 and VC-2A, about 8 km further north (Figure 1; Hulen et al., in press), have encountered strongly altered and locally mineralized hydrothermal breccia zones.

Genetically linking the VC-1 hydrothermal breccias with development of the Valles caldera complex constrains not only their age, but also their depth of formation. The oldest deposits of the caldera complex, the Lower Tuffs of Nielson and Hulen (1984), are believed to range in age from 3.0 to 1.45 Ma (Self et al., 1986). However, the deep brecciation is much more likely to have accompanied (or followed) formation of the Valles caldera (1.12 Ma; Self et al., 1986) or its precursor, the Toledo caldera (1.45 Ma; Self et al., 1986). An upper age limit of brecciation is provided by the unaltered, post-breccia, 0.13-0.6 Ma rhyolitic volcanic sequence penetrated in the upper 305 m of VC-1 (Figure 2).

Since this young rhyolitic sequence had not yet been emplaced, the land surface at the time of brecciation would have been at an elevation of about 2160 m, or about 300 m lower than at present. It is also assumed that the contemporaneous water table was at or near that paleo-surface. Hydrothermal breccias in VC-1 are presently situated between depths of 831.3 m and 849.5 m (Figure 3). If they have not been displaced since formation, the breccias developed at an original depth of about 530 m.

Location of the breccias with a branch of the Jemez fault zone adjacent to the Valles caldera also implies the state of stress at the time of brecciation. Aldrich and Laughlin (1984) have shown that the Jemez fault zone has undergone exclusively normal movement since 7-4 Ma, implying regional extension. Tectonism accompanying formation of the Valles caldera complex was also extensional (Smith and Bailey, 1968) in the shallow interval under discussion. Therefore, an extensional stress field prevailed along the Jemez fault zone prior to and during formation of the VC-1 hydrothermal breccias. In situ stress measurements along the Jemez fault zone by Aldrich and Laughlin (1984) suggest that at the time of brecciation (as now) the least principal regional stress axis was horizontal and oriented NW-SE; the greatest principal stress axis was vertical. These stress orientations are in accordance with steep southeast dips measured both regionally along the Jemez fault zone (Goff and Kron, 1980) and on faults and fractures in the VC-1 core.

In an extensional tectonic environment, a rock will fail by hydraulic rupture when total fluid pressure exceeds only the effective least principal stress, $sigma_x$, by an amount equal to the rock's tensile strength, T (Hubbert and Willis, 1957; Phillips, 1972; Grindley and Browne, 1976; Fournier, 1983). Hubbert and Willis (1957) have shown that in such a regime, $sigma_x$ is horizontal and approximately equal to one third the lithostatic load, S_z, less the normal hydrostatic fluid pressure, P. Assuming an average rock density of 2.7 g/cm^3, and

hydrostatic pressures approximating those of the boiling point vs. depth curve at the time of brecciation, then S_z would have been about 14.1 MPa, P about 4.5 MPa, $sigma_z$ about 9.7 MPa, and $sigma_x$, the least principal effective stress, about 3.2 MPa. Adding a reasonable range of rock tensile strengths (2.1-3.1 MPa; Grindley and Browne, 1976) to this value yields the theoretical total fluid pressure range, 5.3-6.3 MPa, within which the VC-1 rock would have failed by hydraulic rupture.

Actual pressures measured during hydrofracturing experiments at the nearby Fenton Hill Hot Dry Rock site (Figure 1) closely correspond to those theoretically determined. At a depth of 3530 m in a deep Fenton Hill borehole, a pressure of 41.4 MPa (0.0117 MPa/m) was required to induce hydrofracturing (Dash et al., 1985). Multiplying this measured pressure gradient by the assumed depth of brecciation at the VC-1 site (530 m) yields an independent estimate of the pressure required for hydrothermal brecciation--about 6.2 MPa.

Pressure gradients corresponding to lithostatic, boiling hydrostatic, and hydrofracturing pressures can be combined with thermodynamic data from the steam tables of Keenan et al. (1978) to prepare a family of boiling point vs. depth curves which graphically define the physical conditions of hydrothermal brecciation at the VC-1 site (Figure 12). All curves are Figure 12 near here adjusted for elevation of the land surface at the time of brecciation (about 2160 m) and assume water saturation up to that

surface. Although technically valid only for pure water, these curves differ little from those appropriate for the dilute fluids believed responsible for the brecciation. Values plotting to the left of curve FR (Figure 12), the boiling point vs. depth curve at the pressure required to hydrofracture, represent the liquid phase below the threshold fracturing pressure; those to the right represent vapor at pressures exceeding this threshold. It is implicit in this analysis that the Jemez fault zone was hydrothermally sealed prior to each episode of hydrothermal brecciation. In an unsealed conduit, the VC-1 fluids would not have exceeded boiling hydrostatic pressures. An increase in temperature at a given depth would only have induced more vigorous boiling, buffering temperatures and pressures at those appropriate for the hydrostatic boiling point vs. depth curve ("H" on Figure 12).

It is clear from Figure 12 that fluids circulating in the Jemez fault zone, an extensional tectonic feature, could never have achieved lithostatic pressures at the time of hydrothermal brecciation. Rock failure would have been induced at the much lower pressures of curve FR. There are two end-member paths along which this failure could have been effected. Path AB represents hydrofracturing in response to a temperature increase. As the fluid is heated along this path, its vapor pressure eventually exceeds that required to hydrofracture, and the rock ruptures hydraulically; large overpressures are unlikely, since even small fracturing events will buffer pressures at or below

those of curve FR. Hydraulic fracturing due to a rapid release in confining pressure is symbolized by path AC (Figure 12). Such a pressure release at the VC-1 site could have been effected by seismic cracking of a hydrothermally sealed portion of the Jemez fault zone. In this case, extreme overpressures and violent rock disruption are much more likely than along path AB. For example, a fluid at the assumed depth of brecciation, if just below the critical temperature (278°C) and pressure (6.2 MPa) required to hydrofracture, if suddenly depressurized to boiling hydrostatic values through opening of an overlying hydrothermal seal, would be overpressured by about 1.8 MPa. Overpressures of this magnitude may be responsible for the fluidized textures locally common in the hydrothermal breccias of VC-1. These breccias may even have vented to the surface, forming hydrothermal explosion craters such as those of the active geothermal systems at Yellowstone National Park (Muffler et al., 1971) and Waiotapu, New Zealand (Hedenquist and Henley, 1985). Although there is no evidence that the VC-1 breccias vented, neither is there evidence to preclude this possibility.

DISCUSSION AND CONCLUSIONS

The deep breccias of VC-1 have complex multiple origins, not surprising in view of the corehole's location in a long-active fault zone adjacent to a major caldera complex hosting high-temperature geothermal systems. Tectonic breccias of the Jemez fault zone apparently have localized subsequent hydrothermal

brecciation. The age of this brecciation must be inferred, but geologic evidence strongly suggests that rock rupture was induced by hydrothermal fluid overpressuring during multiple hydrothermal episodes accompanying development of the late Cenozoic Valles caldera complex.

Fluid-inclusion characteristics, when studied in conjunction with alteration assemblages and textures as well as the geologic history of the VC-1 site, can be used to deduce the mechanisms of hydrothermal brecciation. For example, all homogenization temperatures for low-salinity fluid inclusions, when plotted at the assumed depth of brecciation, exceed temperatures defining the hydrostatic boiling point vs. depth curve for pure water (curve "H"; Figure 13). This relationship supports the Figure 13 near here supposition that at the VC-1 site, the Jemez fault zone was hydrothermally sealed prior to each episode of brecciation, allowing pressures to approach and intermittently exceed those of curve FR. Hydrothermal brecciation, then, was triggered through a rapid release in confining pressure or renewed heating. Boiling which produced and accompanied this brecciation is documented by coexisting, liquid- and vapor-rich, low-salinity fluid inclusions.

Once the boiling point was exceeded, flashing of these dilute fluids in fractures and intergranular pores ruptured and comminuted enclosing rocks. In some cases, the resulting three-phase mixture (liquid + vapor + solid rock) was involved in

fluidization, with further attrition of entrained rock particles. The increased surface area of these comminuted fragments facilitated hydrothermal alteration.

Homogenization temperatures of high-salinity fluid inclusions, when plotted at the same mean depth of brecciation at the VC-1 site (Figure 14), by contrast with those of coexisting

Figure 14 near here

dilute inclusions are well below temperatures and pressures defining a corresponding hydrostatic boiling point curve. This relationship clearly indicates that these saline fluids were not involved in the hydrothermal brecciation recorded by their dilute counterparts.

The occurrence of molybdenite in the hydrothermal breccias of VC-1 further strengthens the supposition that they are genetically related to the Valles caldera complex. The only other reported occurrence of this sulfide in the Jemez Mountains is in young (<1.12 Ma) intracaldera tuffs penetrated by CSDP corehole VC-2A, at Sulphur Springs in the Valles caldera (Fig. 1; Hulen et al., in press). Molybdenite in the Sulphur Springs rocks, like that of VC-1, is intimately associated with hydrothermal brecciation and intense phyllic alteration. Hydrothermal phengite, an uncommon layer silicate abundant in the VC-1 breccias, is also common in VC-2A.

The shallow molybdenum mineralization intersected in VC-2A is very similar to that occurring above some deeply concealed, Climax-type, stockwork molybdenite deposits (Hulen et al., in

review). The molybdenite, associated alteration and hydrothermal brecciation penetrated in VC-1 and VC-2A could represent high-level leakage from a deep, Climax-type hydrothermal system.

Our studies of the two Valles CSDP coreholes have shown that, as in many New Zealand geothermal systems (Grindley and Browne, 1976; Hedenquist and Henley, 1985), hydraulic fracturing and hydrothermal brecciation have created or enhanced structural permeability in high-temperature geothermal systems of the Valles caldera. Discovery of these hydraulically fractured and brecciated rocks, not recognized from previous studies bases on rotary drill cuttings, exemplifies the value of continuous core from carefully monitored scientific drilling.

ACKNOWLEDGEMENTS

This research was made possible by grant number FE-FG02-86ER13467.M001 from the Office of Basic Energy Sciences of the U.S. Department of Energy. XRD samples and diffractograms were prepared by Louise McPherson. Core photographs are the work of the Medical Illustrations Department of the University of Utah Medical Center. We thank M. C. Adams, F. E. Goff, T.E.C. Keith, and P.R.L. Browne for their careful and extremely helpful reviews.

REFERENCES

Aldrich, M.J., and A.W. Laughlin, A model for the tectonic development of the southeastern Colorado Plateau boundary, J. Geophys. Res., 89, 10207-10218, 1984.

Armstrong, A. K., and B. L. Mamet, Biostratigraphy of the Arroyo Penasco Group, Lower Carboniferous (Mississippian), north-central New Mexico, New Mexico Geol. Soc. Guidebook, 25th Field Conf., Ghost Ranch (Central-Northern New Mexico), pp. 145-158, 1974.

Baars, D. L., and G. M. Stevenson, The San Luis uplift, Colorado and New Mexico--an enigma of the Ancestral Rockies, The Mountain Geologist, 21, 57-67, 1984.

Berger, B. R., Geologic-geochemical features of hot-spring precious metal deposits in Geologic characteristics of sediment- and volcanic-hosted disseminated gold deposits--search for an occurrence model, edited by E. W. Tooker, U.S. Geol. Survey, Bull. 1646, 47-54, 1985.

Burruss, R. C., and L. S. Hollister, Evidence from fluid inclusions for a paleogeothermal gradient at the geothermal test well sites, Los Alamos, New Mexico, J. Volc. and Geoth. Res., 5, 163-177, 1979.

Dash, Z.V., D.S. Dreesen, F. Walter, and L. House, The massive hydraulic hydrofracture of Fenton Hill HDR well EE-3, Geoth. Res. Council Trans., 9, pt. II,83-88, 1985.

Doell, R. R., G. B. Dalrymple, R. L. Smith, and R. A. Bailey, Paleomagnetism, potassium-argon ages, and geology of rhyolites and associated rocks of the Valles caldera, New Mexico in Studies in volcanology, edited by R. R. Coats, R. L. Hay, and C. A. Anderson, Geol. Soc. America Mem. 116, 211-248, 1968.

DuChene, H. R., Pennsylvanian rocks of north-central New Mexico, New Mexico Geol. Soc. Guidebook, 25th Field Conf., Ghost Ranch (Central-Northern New Mexico), pp. 159-165, 1974.

Dunoyer de Segonzac, G., The transformation of clay minerals during diagenesis and low-grade metamorphism--a review, Sedimentology, 15, 281-346, 1970.

Fitzsimmons, J. P., A. K. Armstrong, and G. MacKenzie, Jr., Arroyo Penasco Formation, Mississippian, north-central New Mexico, American Assoc. Pet. Geol. Bull., 40, 1935-1944, 1956.

Gardner, J. N., F. Goff, S. Garcia, and R. C. Hagan, Stratigraphic relations and lithologic variation in the Jemez volcanic field, New Mexico, J. Geophys. Res., 91, 1763-1778, 1986.

Goff, F. E., C. O. Grigsby, A. Kron, D. Counce, and P. Trujillo, Jr., Geology and geothermal potential of the Jemez Springs area, Canon de San Diego, New Mexico, J. Volc. and Geoth. Res., 10, 227-244, 1981.

Goff, F., and A. Kron, In-progress geologic map of Canon San Diego, Jemez Springs, New Mexico, and lithologic log of Jemez Springs geothermal well, Los Alamos Scientific Laboratory, Map LA-8276-MAP, 1980.

Goff, F., J. Rowley, J. N. Gardner, W. Hawkins, S. Goff, R. Charles, D. Wachs, L. Maassen, and G. Heiken, Initial results from VC-1, first Continental Scientific Drilling Program Corehole in Valles caldera, New Mexico, J. Geophys. Res., 91, 1742-1752, 1986.

Gordon, C. H., Notes on the Pennsylvanian Formations in the Rio Grande Valley, New Mexico, J. Geol., 15, 805-816, 1907.

Grindley, G.W., and P.R.L. Browne, Structural and hydrologic factors controlling the permeabilities of some hot-water geothermal fields, Proc. 2nd U. N. Symp. on Devel. and Use of Geoth. Resources, 1, San Francisco, pp. 377-386, 1976.

Haas, J.L., The effect of salinity on the maximum thermal gradient of a hydrothermal system at hydrostatic pressure, Econ. Geology, 66, 940-946, 1971.

Hedenquist, J.W., and R. W. Henley, Hydrothermal eruptions in the Waiotapu geothermal system, New Zealand: Their origin, associated breccias, and relation to precious metal mineralization, Econ. Geol., 80, 1640-1668, 1985.

Heiken, G., F. Goff, J. Stix, S. Tamanyu, M. Shafiqullah, S. Garcia, and R. Hagan, Intracaldera volcanic activity, Toledo caldera and embayment, Jemez Mountains, New Mexico, J. Geophys. Res., 91, 1799-1815, 1986.

Hubbert, M.K. and D.G. Willis, Mechanics of hydraulic fracturing, American Inst. Mining, Metal., and Petrol. Eng. Trans., 210, 153-166, 1957.

Hulen, J. B., and D. L. Nielson, Stratigraphic permeability in the Baca geothermal system, Redondo Creek area, Valles caldera, New Mexico, Geoth. Res. Counc. Trans., 6, 27-30, 1982.

Hulen, J. B., and D. L. Nielson, Altered tectonic and hydrothermal breccias in corehole VC-1, Valles caldera, New Mexico (abs.), EOS, 66, 1081, 1985.

Hulen, J. B., and D. L. Nielson, Hydrothermal alteration in the Baca geothermal system, Redondo dome, Valles caldera, New Mexico, J. Geophys. Res., 91, 1867-1886, 1986a.

Hulen, J. B. and D. L. Nielson, Stratigraphy and hydrothermal alteration in well Baca-8, Sulphur Springs area, Valles caldera, New Mexico, Geoth. Res. Counc. Trans., 10, 187-192, 1986b.

Hulen, J. B., D. L. Nielson, F. Goff, J. N. Gardner, and R. W. Charles, Molybdenum mineralization in an active geothermal system, Valles caldera, New Mexico, Geology, in press.

Izett, G. A., J. D. Obradovich, C. W. Naeser, and G. T. Cebula, Potassium-argon and fission-track zircon ages of Cerro

Toledo rhyolite tephra in the Jemez Mountains, New Mexico, U. S. Geol. Survey Prof. Pap. 1199-D, pp. 37-43, 1980.

Keenan, J.H., F.G. Keyes, P.G. Hill, and J.G. Moore, Steam tables and thermodynamic properties of water including vapor, liquid, and solid phases, New York, John Wiley & Sons, 156 pp., 1978.

Keith, T.E.C., Alteration in the Madera Limestone and Sandia Formation from core hole VC-1, Valles caldera, New Mexico, J. Geophys. Res., this issue.

Kelley, V. C., and S. A. Northrop, Geology of Sandia Mountains and vicinity, New Mexico, New Mex. Bur. Mines and Min. Res. Mem. 29, 136 pp., 1975.

Lehrman, N. J., Geology and geochemistry of the McLaughlin hot-spring precious-metal deposit, California coast ranges (abs), Geol. Soc. Nev., Symp. on Bulk Mineable Precious Metal Deposits of the Western United State, Abs. with Prog., Sparks, Nev., p. 44, 1987.

Leonardson, R. W., G. Dunlop, V. L. Starquist, G. Bratton, J. W. Meyer, L. W. Osborne, S. A. Atkin, P. A. Molling, R. F. Moore and S. D. Olmore, Preliminary geology and molybdenum deposits at Questa, New Mexico, in The genesis of Rocky

Mountain ore deposits--changes with time and tectonics, Golden, Colorado, Denver Region Expl. Geol. Society Proc., pp. 151-155, 1983.

Laughlin, A. W., The geothermal system of the Jemez Mountains, New Mexico and its exploration in Geothermal systems--principles and case histories, edited by L. Rybach and L. J. P. Muffler, New York, John Wiley and Sons, pp. 295-320, 1981.

Loughlin, G. H., and A. H. Koschmann, Geology and ore deposits of the Magdalena mining distirct, New Mexico, U. S. Geol. Survey Prof. Pap. 200, 168 pp., 1942.

McCallum, M. E., Experimental evidence for fluidization processes in breccia pipe formation, Econ. Geol., 80, 1523-1543, 1985.

Muffler, L.J.P., D.E. White, and A.H. Truesdell, Hydrothermal explosion craters in Yellowstone National Park, Geol. Soc. America Bull. 82, 723-740, 1971.

Mutschler, F.E., E.G. Wright, S. Ludington, and J.T. Abbott, Granite molybdenite systems, Econ. Geol., 76, 874-897.

Nielson, D.L., and J.B. Hulen, Internal geology and evolution of

the Redondo Dome, Valles caldera, New Mexico, J. Geophys. Res., 89, 8695-8712, 1984.

Phillips, W.J., Hydraulic fracturing and mineralization, J. Geol. Soc. London, 128, 337-359, 1972.

Potter, R.W., Pressure corrections for fluid-inclusion homogenization temperatures based on the volumetric properties of the system NaCl-H_2O, J. Res. U. S. Geol. Survey, 5, 603-607, 1977.

Reynolds, D.L., Fluidization as a geological process, and its bearing on the problem of intrusive granites, Am. Jour. Sci., 252, 557-613, 1954.

Reynolds, R.C., Interstratified clay minerals, in Crystal structures of clay minerals and their X-ray identification Min. Soc. London Mon. 5, 249-304, 1980.

Roedder, E., Fluid inclusions, Min. Soc. America, Rev. in Mineralogy, 12, 644 pp., 1984

Sasada, M., Microthermometry of fluid inclusions from the VC-1 core hole in Valles caldera, New Mexico, J. Geophys. Res., this issue.

Self, S., F. Goff, J.N., Gardner, J.V. Wright, and W.M. Kite, Explosive rhyolitic volcanism in the Jemez Mountains--vent locations, caldera development and relation to regional structure, J. Geophys. Res., 91, 1779-1798, 1986.

Shevenell, L., F. Goff, F. Vuataz, R. Trujillo, D. Counce, C. Janik and W. Evans, Hydrochemical data for thermal and nonthermal waters and gases of the Valles caldera-southern Jemez Mountains region, New Mexico, Los Alamos Nat. Lab. Rept. LA-10923-OBES, 100 pp., 1987.

Sibson, R.H., Fault rocks and fault mechanisms, J. Geol. Soc. London, 133, 191-213, 1977.

Siemers, W.T., The Pennsylvanian system, Socorro region, New Mexico--stratigraphy, petrology, depositional environments, New Mexico Geol. Soc. Guidebook, 34th Field Conf. (Socorro Region II), pp. 147-155, 1983.

Sillitoe, R.H., Ore-related breccias in volcanoplutonic arcs, Econ. Geol., 80, 1467-1514, 1985.

Smith, R.L. and R.A. Bailey, Resurgent cauldrons, in Studies in Volcanology, edited by R.R. Coats, R.L. Hay, and C.A. Anderson, Geol. Soc. America Mem. 116, pp. 613-632.

Srodon, J., Precise identification of illite/smectite interstratifications by X-ray powder diffraction, Clays and Clay Minerals, 28, 401-411, 1980.

Truesdell, A.H. and R.O. Fournier, Calculation of deep temperatures in geothermal systems from the chemistry of boiling spring waters of mixed origin, Proc. 2nd U. N. Symp. on Devel. and Use of Geoth. Res., 1, San Francisco, pp. 837-844, 1976.

Truesdell, A.H. and C.J. Janik, Reservoir processes and fluid origins in the Baca geothermal system, Valles caldera, New Mexico, J. Geophys. Res., 91, 1817-1833, 1986.

Vuataz, F.D. and F. Goff, Isotope geochemistry of thermal and nonthermal waters in the Valles caldera, Jemez Mountains, northern New Mexico, J. Geopys. Res., 91, 1835-1853, 1986.

White, W.H., A.A. Bookstrom, R.J. Kamilli, M.W. Ganster, R.P. Smith, D.E. Ranta, and R.C. Steininger, Character and origin of Climax-type molybenum deposits, Econ. Geol., 75th Ann. Vol., pp. 270-316, 1981.

Wronkiewicz. D., D. Norman, G. Parkison, and K. Emanuel, Geology of the Cochiti mining district, Sandoval County, New Mexico, New Mexico Geol. Soc. Guidebook, 35th Field Conf., pp. 219-222, 1984.

Figure Captions

Figure 1. Location map, showing position of CSDP corehole VC-1 relative to the Valles caldera complex and the Jemez fault zone in north-central New Mexico.

Figure 2. Generalized stratigraphic and temperature log for corehole VC-1. Tectonic and hydrothermal breccia interval discussed in this paper spans the depth range 826-856 m. Modified from Goff et al. (1986).

Figure 3. Detailed lithologic and hydrothermal alteration log of the lower portion of corehole VC-1 (806-856.1 m), showing tectonic and hydrothermal breccia intercepts. Downhole histograms at right display distributions of rock-forming and alteration phases as determined by bulk XRD analysis. Actual values shown by black bars; stippling between bars added only for clarity. AB--albite; FLT--fault; FM--formation; FSP--feldspar; HEM--hematite; KF--potassium feldspar; LITH--lithology; MoS_2--molybdenite.

Figure 4. Quartz-sericitized, intensely fractured, Precambrian granitic orthogneiss from the depth

interval 842.8-842.9 m (top to left). Note relict gneissic foliation inclined to the right at about 45° to the core axis. Q--quartz veinlet; PY--disseminated pyrite.

Figure 5. Shaly, hematitic, tectonically rebrecciated sedimentary breccia from the depth interval 829.6-829.7 m (top to left). Note prominent shearing of the matrix. CTBX--recrystallized, sparsely chloritic chert breccia clast cut by hydrothermal quartz veinlet truncated at clast margins;

Figure 6. Portion of a mineralized, dolomitic limestone breccia clast in hydrothermal breccia from the depth interval 831.8-831.9 m (top to left). Breccia texture of the clast partially obscured by recrystallization of carbonates. Dark grains are disseminated, post-breccia, hydrothermal magnetite, pyrite and rare hematite. White clasts are disrupted, pre-breccia hydrothermal barite.

Figure 7. Shaly, carbonate-rich, matrix-dominated tectonic breccia from the depth interval 850.4-850.5 m (top to left). CHT--recrystallized, sparsely chloritic chert clasts; GN--hydrothermally altered, phengite-rich clasts of Precambrian gneiss; LS--

recrystallized limestone clasts. Note anastamosing, late-stage, chlorite-calcite veinlets.

Figure 8. Altered hydrothermal breccia from the depth interval 847.6-847.7 m (top to left). Clasts consist of quartz-sericitized gneiss and sandstone, rare chert, and older breccias incorporating one or more of these rock types. Dark matrix is rock flour altered to quartz, illite, phengite and pyrite. Note flow-foliation in matrix, probably developed during fluidization.

Figure 9. Molybdenum-bearing hydrothermal breccia from a depth of 846.7 m, showing prominent flow-foliation in matrix. Also shown is a well-rounded clast of sandstone/gneiss breccia cut by a quartz microveinlet truncated at clast margins, attesting to formation of the veinlet prior to the most recent episode of hydrothermal brecciation. Molybdenite forms sparse, discontinuous microrims on several clasts, but also occurs on late stage fractures.

Figure 10. Plot of homogenization temperatures vs. ice-melting temperatures (freezing point depressions)

for 58 fluid inclusions in quartz from the hydrothermally brecciated interval between depths of 842.9 and 847.7 m. The inclusions form two distinct compositional groups: one characterized by dilute, high-temperature fluids, the other by fluids of moderate temperature and high salinity. Shown for comparison are corresponding data for fluid inclusions in Precambrian crystalline rock above a depth of 1304 m in a deep geothermal well at the Fenton Hill Hot Dry Rock site (Burruss and Hollister, 1979).

Figure 11. Chloride-enthalpy diagram calculated from the fluid-inclusion data presented in Figure 10. Characteristics of Jemez River water from Vuataz and Goff (1986).

Figure 12. Depth vs. temperature plot and boiling point curves calculated for pure water and various relevant pressures at the time of hydrothermal brecciation at the VC-1 site. FR is the boiling point curve at pressures required to hydrofracture. H and L are, respectively, hydrostatic and lithostatic boiling point curves shown for comparison. Originating at the mean depth of brecciation, path AB symbolizes

hydrofracturing due to increased heating. Path AC represents hydraulic rock rupture in response to rapid pressure release.

Figure 13. Depth vs. temperature plot and boiling point curves of Figure 12, showing homogenization temperatures for dilute, probable interbreccia fluid inclusions in the VC-1 hydrothermal breccias. Hatching indicates primary inclusions.

Figure 14. Depth vs. temperature plot and boiling point curve appropriate for fluid of 20% (wt.) salinity (from Haas, 1971) under hydrostatic pressure at the time of brecciation at the VC-1 site, showing homogenization temperatures for high-salinity fluid inclusions in hydrothermal breccias.

FIGURE 1

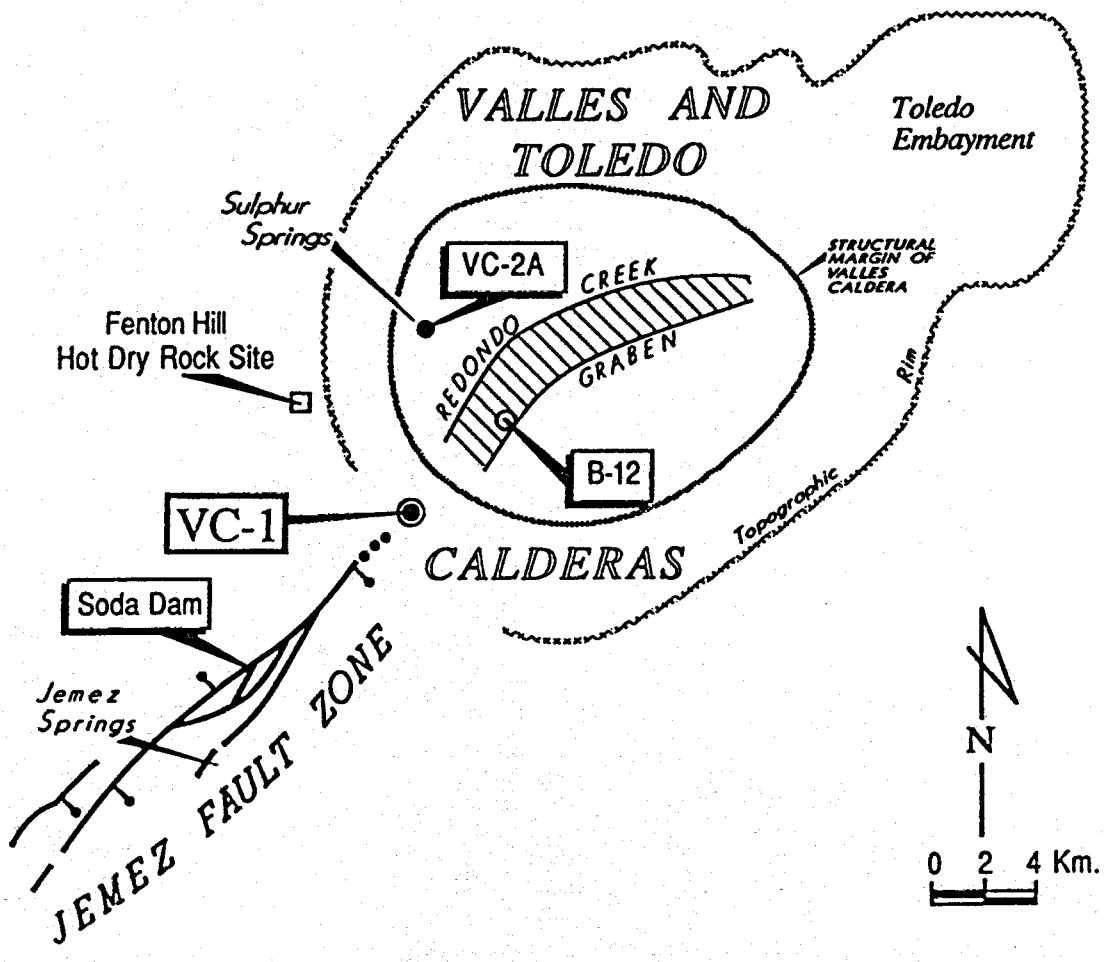
VALLES AND TOLEDO
CALDERAS
Toledo Embayment
Sulphur Springs
VC-2A
CREEK
REDONDO
GRABEN
STRUCTURAL MARGIN OF VALLES CALDERA
Fenton Hill
Hot Dry Rock Site
B-12
VC-1
Topographic Rim
Soda Dam
Jemez Springs
JEMEZ FAULT ZONE
N
0 2 4 Km.

FIGURE 2
(DRAFT)

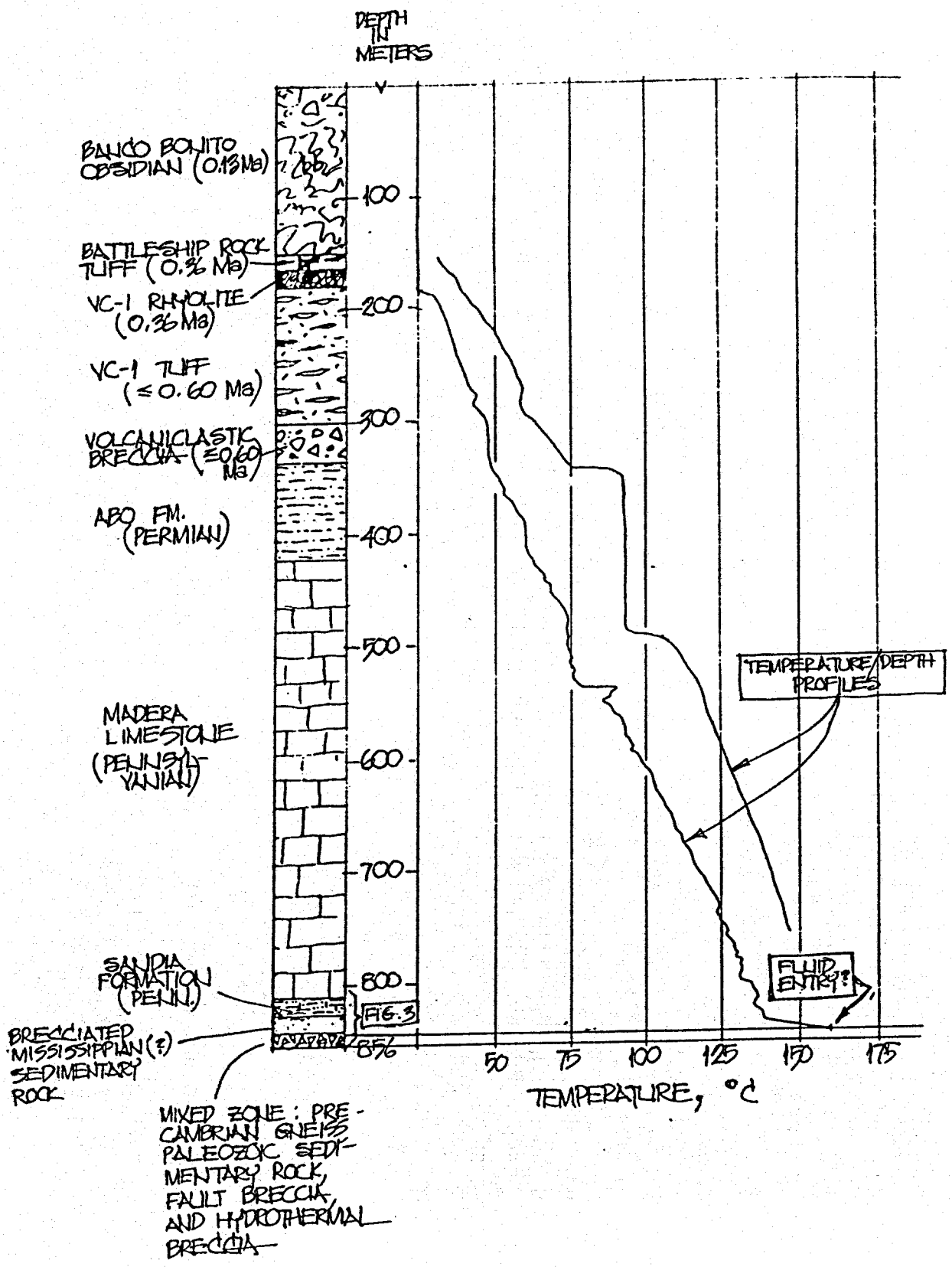

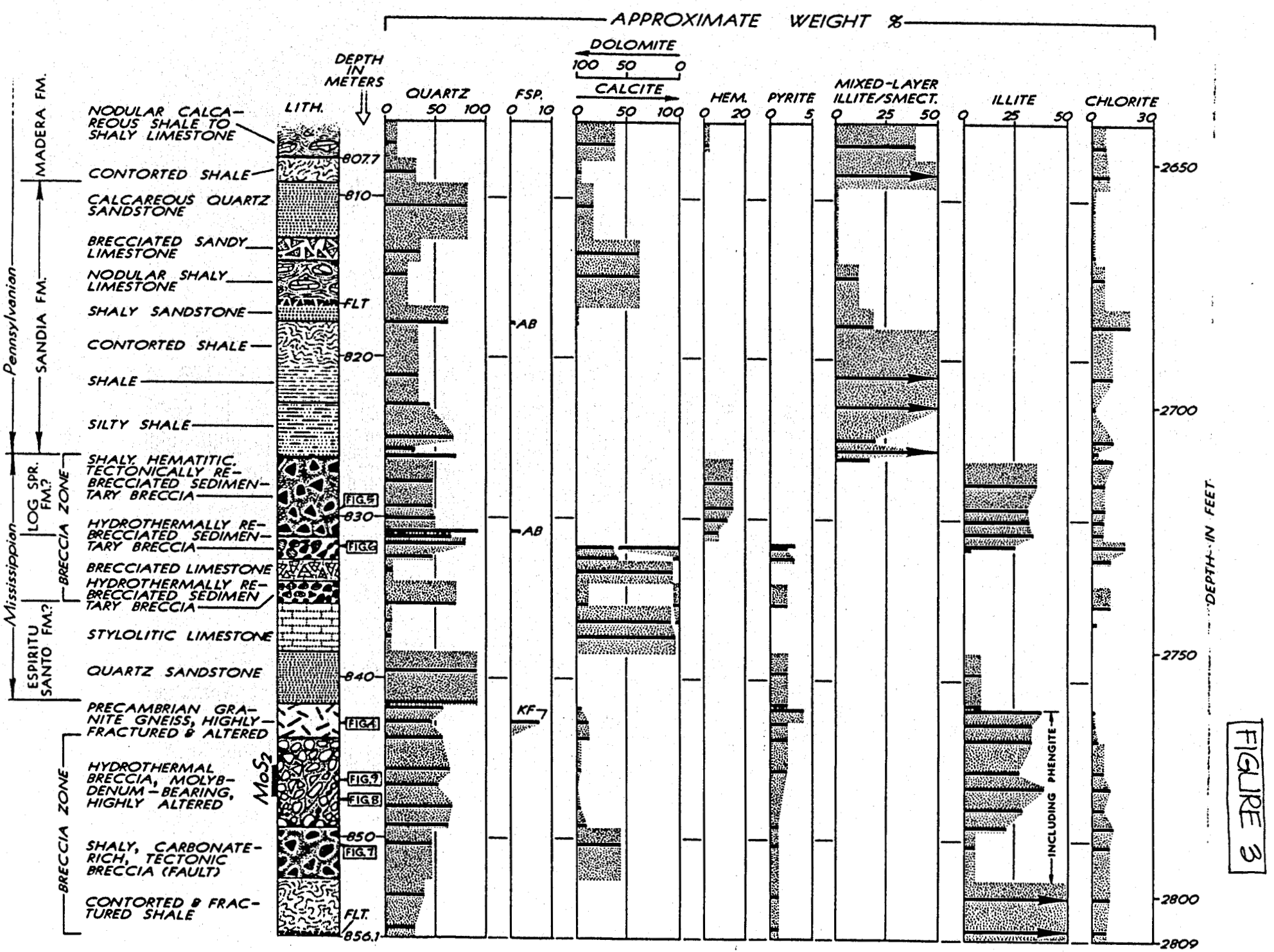
APPROXIMATE WEIGHT %
DEPTH IN METERS
LITH.
QUARTZ
FSP.
DOLOMITE
CALCITE
HEM.
PYRITE
MIXED-LAYER ILLITE/SMECT.
ILLITE
CHLORITE
Pennsylvanian
Mississippian
MADERA FM.
SANDIA FM.
LOG SPR. FM.?
ESPIRITU SANTO FM.?
BRECCIA ZONE
BRECCIA ZONE
NODULAR CALCAREOUS SHALE TO SHALY LIMESTONE
CONTORTED SHALE
CALCAREOUS QUARTZ SANDSTONE
BRECCIATED SANDY LIMESTONE
NODULAR SHALY LIMESTONE
SHALY SANDSTONE
CONTORTED SHALE
SHALE
SILTY SHALE
SHALY, HEMATITIC, TECTONICALLY RE-BRECCIATED SEDIMENTARY BRECCIA
HYDROTHERMALLY RE-BRECCIATED SEDIMENTARY BRECCIA
BRECCIATED LIMESTONE
HYDROTHERMALLY RE-BRECCIATED SEDIMENTARY BRECCIA
STYLOLITIC LIMESTONE
QUARTZ SANDSTONE
PRECAMBRIAN GRANITE GNEISS, HIGHLY FRACTURED & ALTERED
HYDROTHERMAL BRECCIA, MOLYBDENUM-BEARING, HIGHLY ALTERED
MoS2
SHALY, CARBONATE-RICH, TECTONIC BRECCIA (FAULT)
CONTORTED & FRACTURED SHALE
807.7
810
FLT
820
830
840
850
FLT.
856.1
FIG.5
FIG.6
FIG.4
FIG.9
FIG.8
FIG.7
AB
AB
KF
INCLUDING PHENGITE
2650
2700
2750
2800
2809
DEPTH IN FEET

FIGURE 3

FIGURE 4

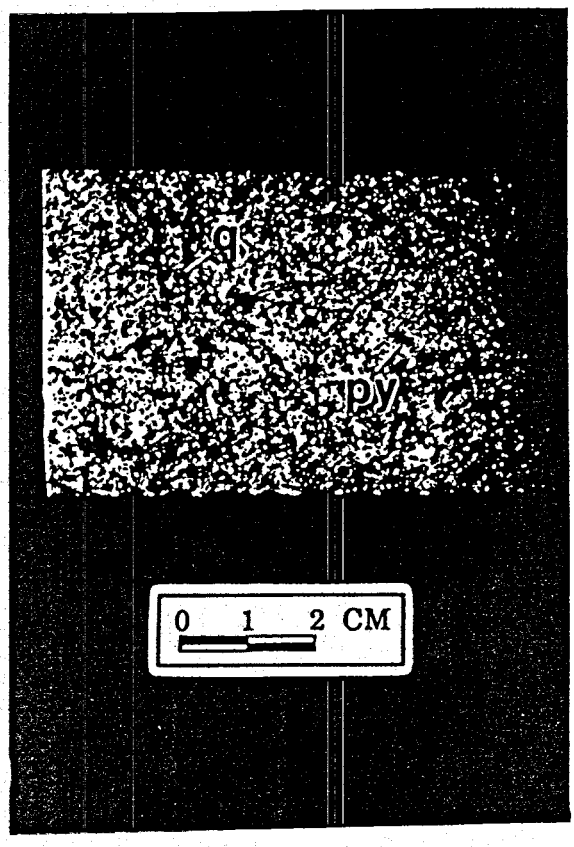

FIGURE 5

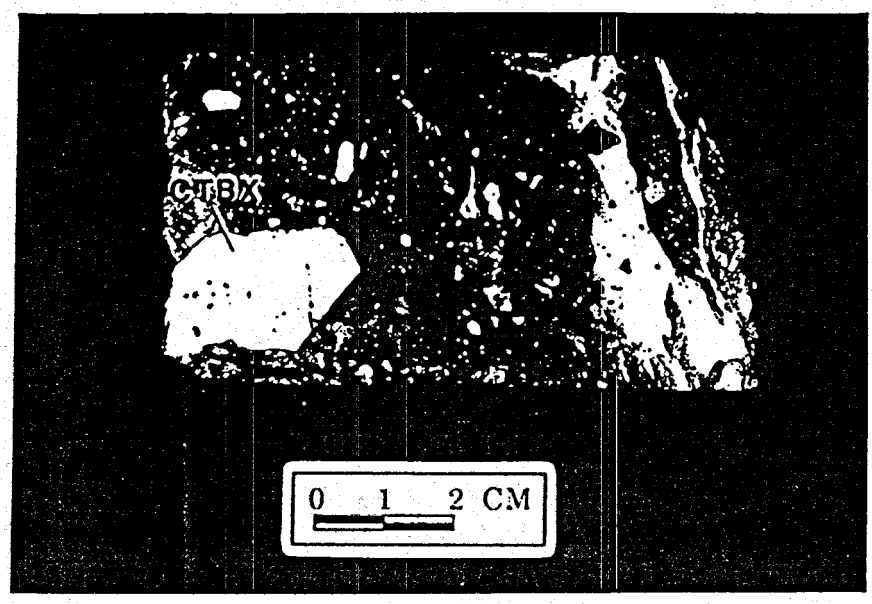

FIGURE 6

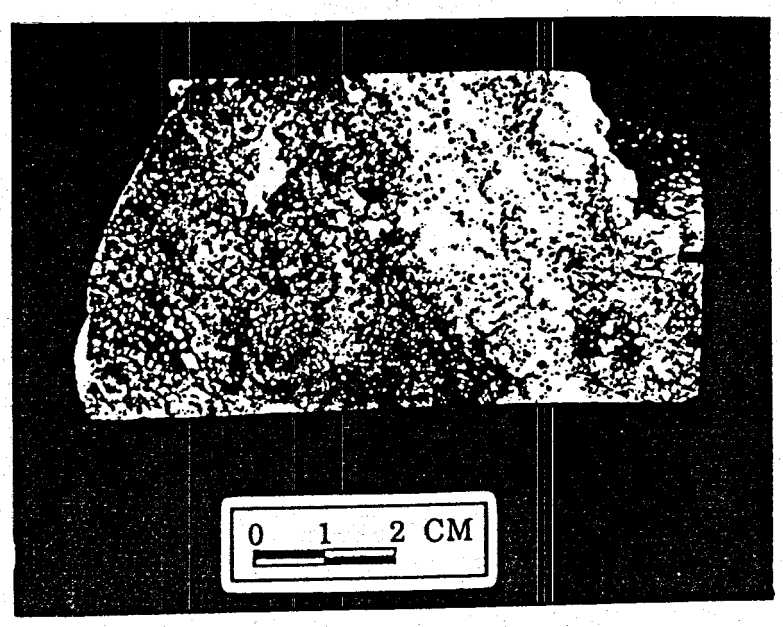

FIGURE 7

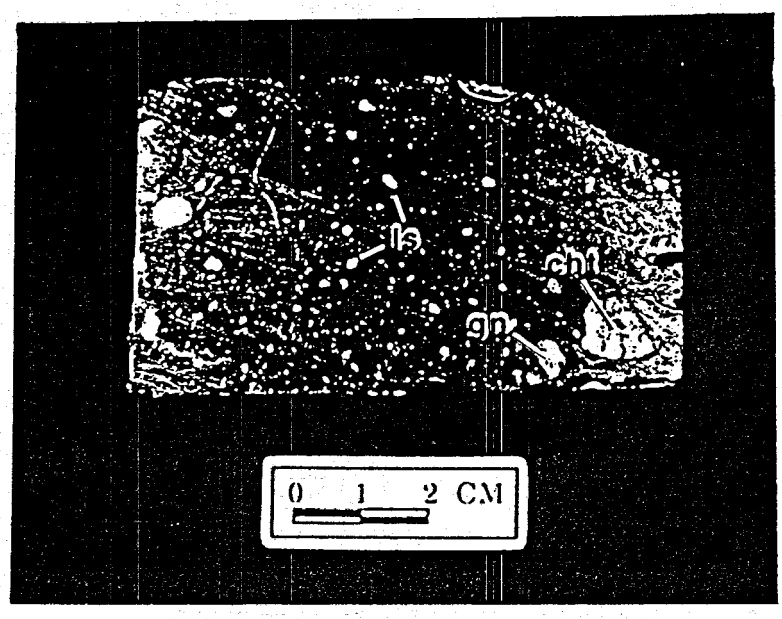

FIGURE 8

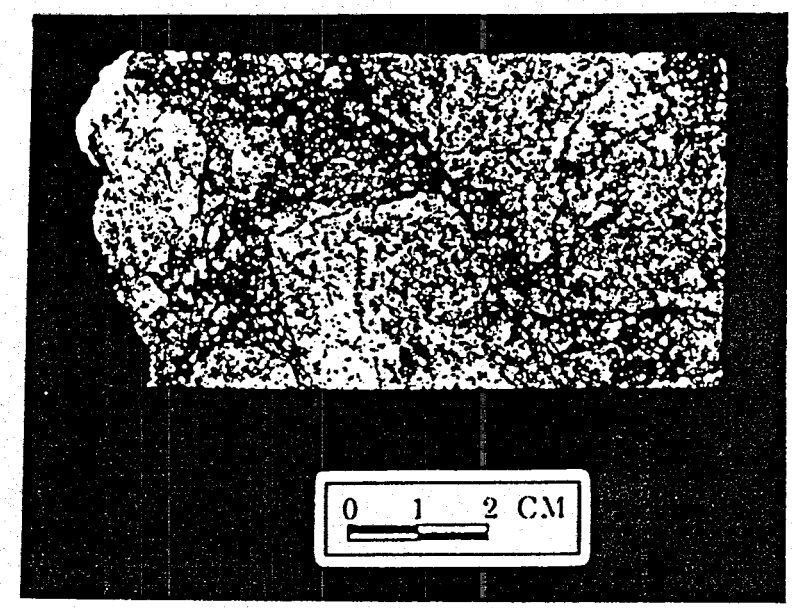

FIGURE 9

FIGURE 10

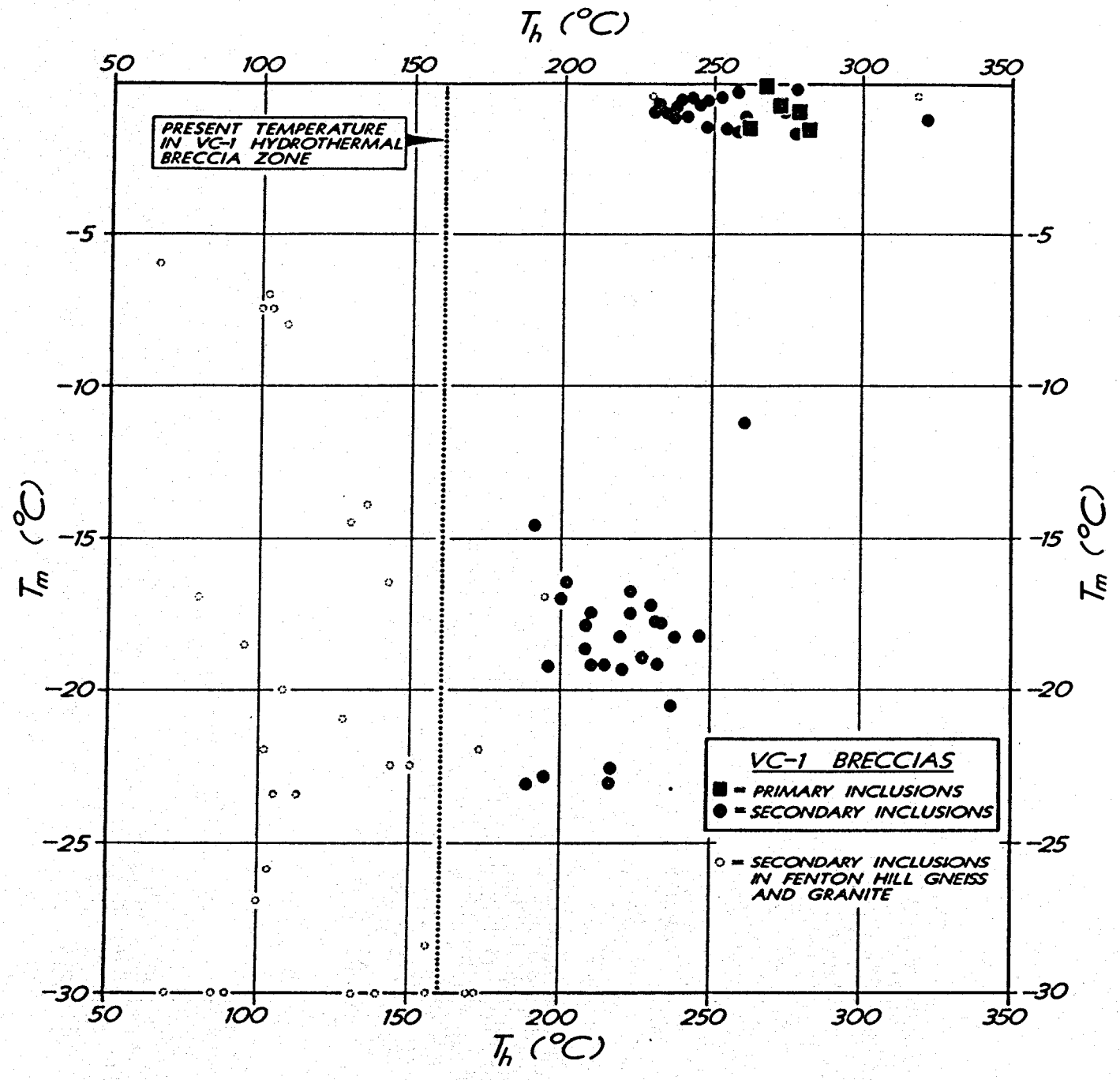
T_h (°C)
50
100
150
200
250
300
350
PRESENT TEMPERATURE IN VC-1 HYDROTHERMAL BRECCIA ZONE
-5
-10
-15
-20
-25
-30
T_m (°C)
VC-1 BRECCIAS
■ = PRIMARY INCLUSIONS
● = SECONDARY INCLUSIONS
○ = SECONDARY INCLUSIONS IN FENTON HILL GNEISS AND GRANITE

FIGURE 11

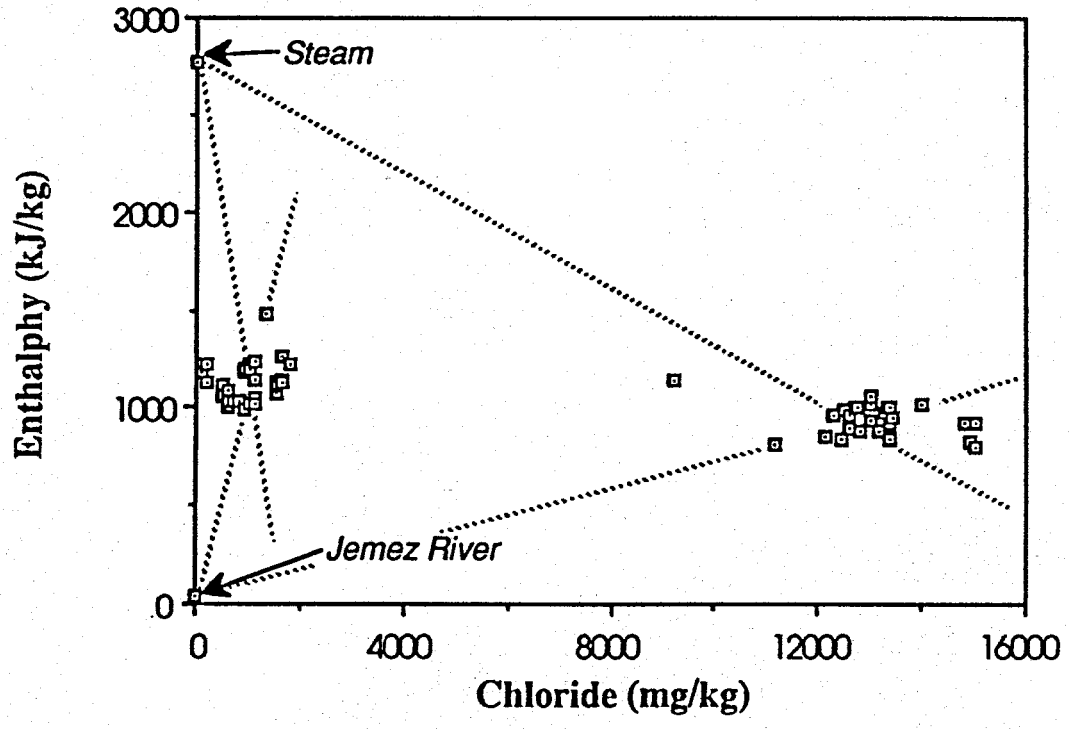
3000
2000
1000
0
Steam
Jemez River
Enthalphy (kJ/kg)
0
4000
8000
12000
16000
Chloride (mg/kg)

FIGURE 12

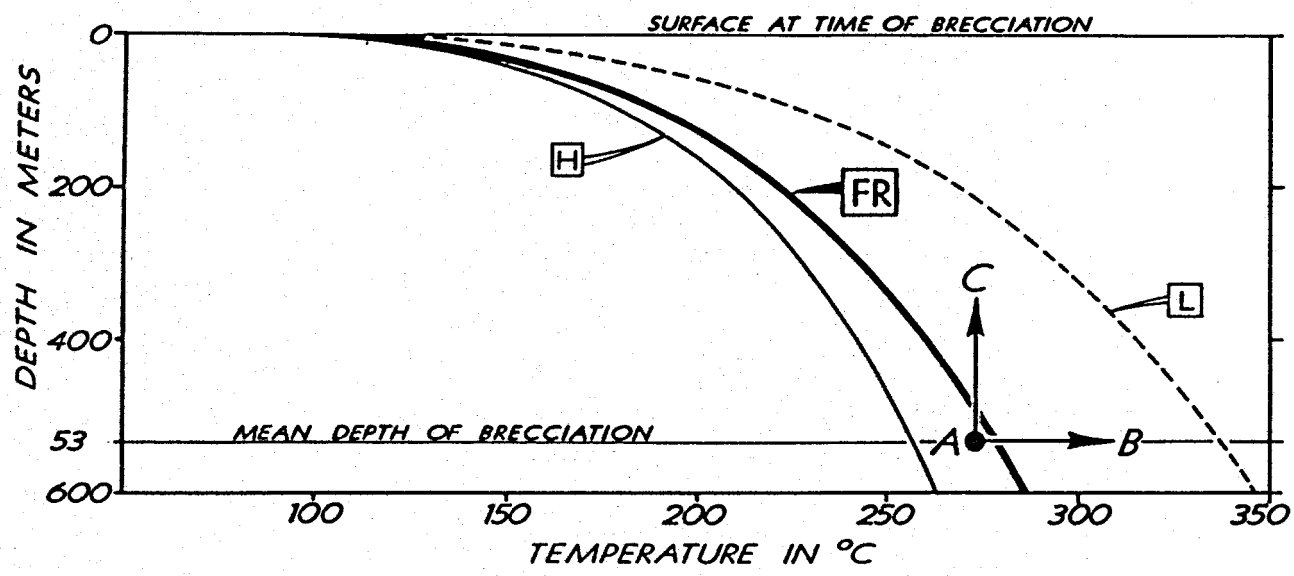
SURFACE AT TIME OF BRECCIATION
0
200
400
53
600
DEPTH IN METERS
H
FR
L
C
A
B
MEAN DEPTH OF BRECCIATION
100
150
200
250
300
350
TEMPERATURE IN °C

FIGURE 13

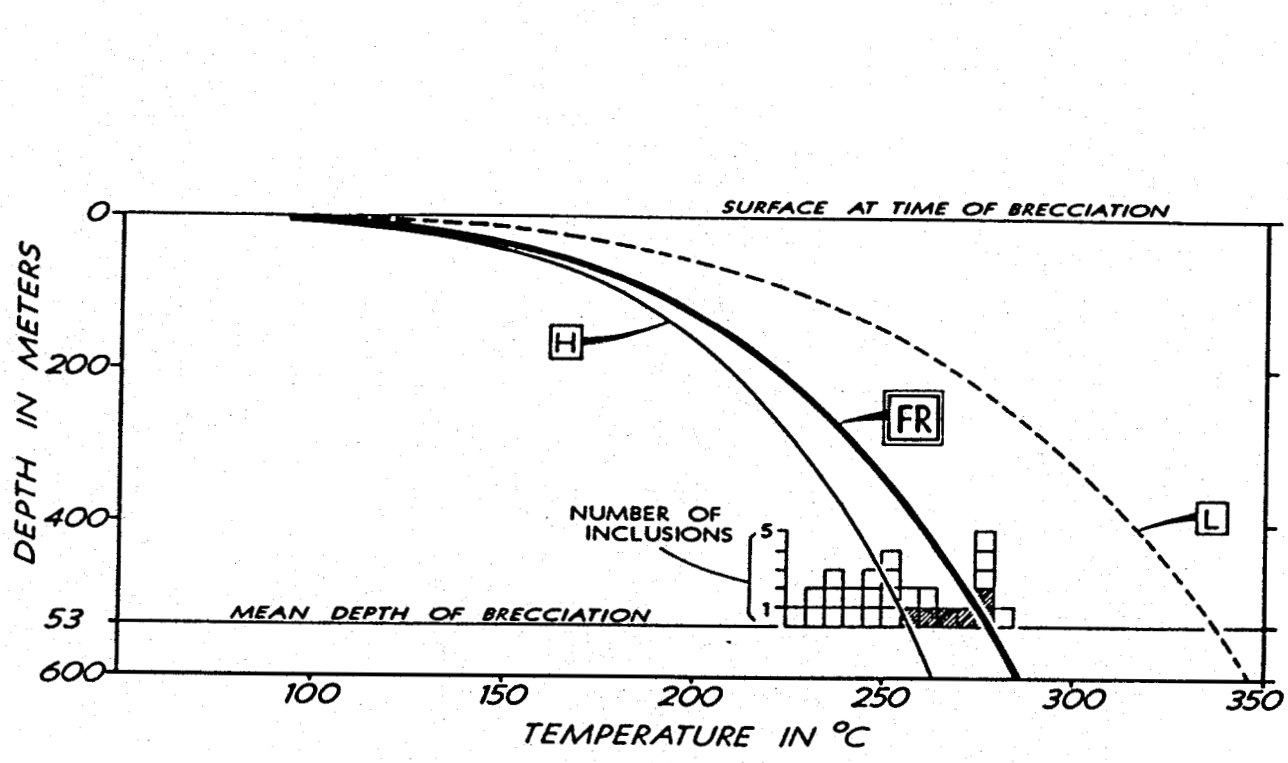
SURFACE AT TIME OF BRECCIATION
0
200
400
53
600
DEPTH IN METERS
H
FR
L
NUMBER OF INCLUSIONS
5
1
MEAN DEPTH OF BRECCIATION
100
150
200
250
300
350
TEMPERATURE IN °C

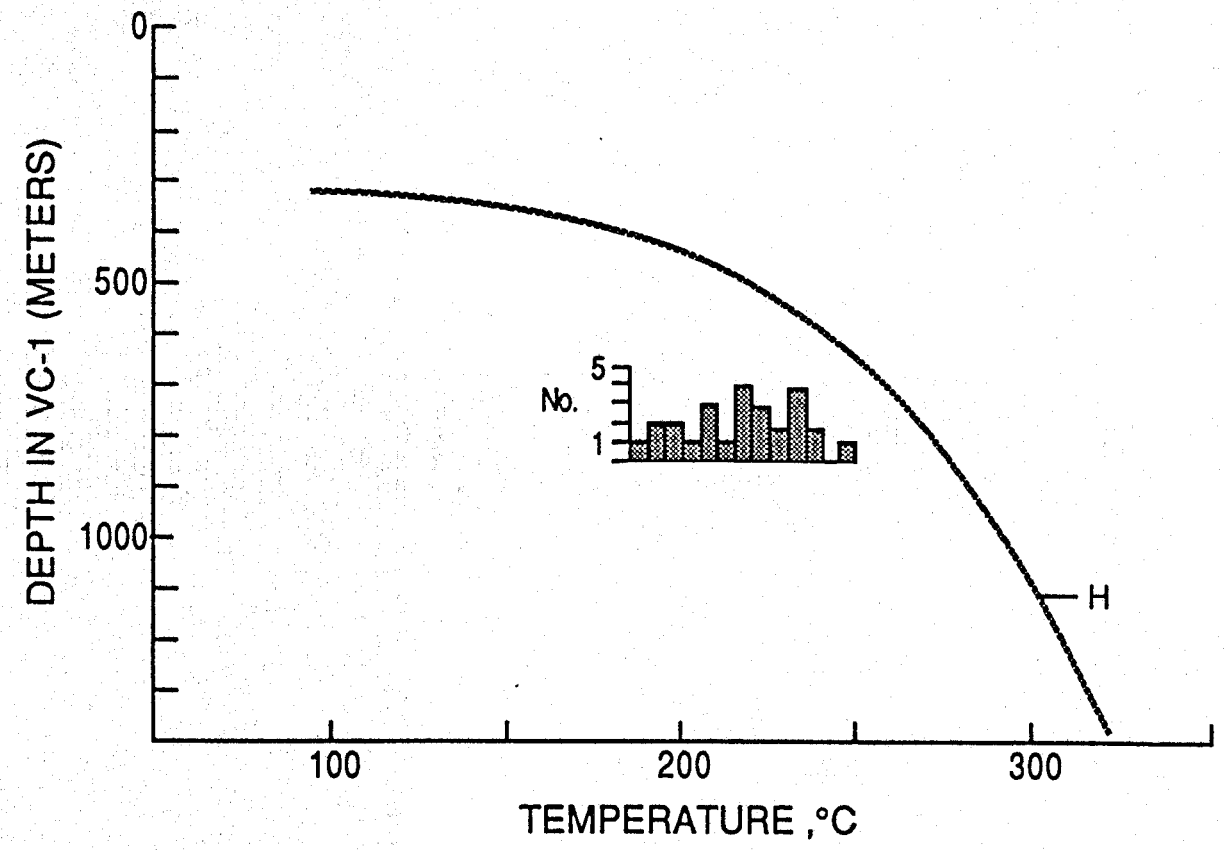

FIGURE 14

(DRAFT: WILL BE MODIFIED TO CONFORM TO FIGS. 12 & 13)